Genetic and pharmacological reduction of CDK14 mitigates α-synuclein pathology in human neurons and in rodent models of Parkinson's disease

Authors: Jean-Louis A. Parmasad[1,2,†], Konrad M. Ricke[1,2,3†], Morgan G. Stykel[4], Brodie Buchner-Duby[4], Benjamin Nguyen[1,2,3], Amanda Bruce[1,2], Haley M. Geertsma[1,2,3], Eric Lian[5,6], Nathalie A. Lengacher[1,3,5], Steve M. Callaghan[1,2,3], Alvin Joselin[7], Julianna J. Tomlinson[1,3,5], Michael G. Schlossmacher[1,3,5], William L. Stanford[2,5,6], Jiyan Ma[8,#], Patrik Brundin[8], Scott D. Ryan[4], and Maxime W.C. Rousseaux[1,2,3,6,*]

Affiliations:

[1] University of Ottawa Brain and Mind Research Institute, Ottawa, ON

[2] Department of Cellular and Molecular Medicine, University of Ottawa, Ottawa, ON

[3] Aligning Science Across Parkinson's (ASAP) Collaborative Research Network, Chevy Chase, MD

[4] Department of Molecular and Cellular Biology, University of Guelph, Guelph, ON

[5] Program in Neuroscience, Ottawa Hospital Research Institute, Ottawa, ON

[6] Ottawa Institute for Systems Biology, University of Ottawa, Ottawa, ON

[7] Hotchkiss Brain Institute, Department of Clinical Neurosciences, University of Calgary, Calgary, AB

[8] Parkinson's Disease Center, Department of Neurodegenerative Science, Van Andel Institute, Grand Rapids, MI

[†]Authors contributed equally

[#]Present address: Chinese Institute for Brain Research, Beijing, China

*Corresponding author. Email: max.rousseaux@uottawa.ca

Abstract:

Parkinson's disease (PD) is a debilitating neurodegenerative disease characterized by the loss of midbrain dopaminergic neurons (DaNs) and the abnormal accumulation of α-Synuclein (α-Syn) protein. Currently, no treatment can slow nor halt the progression of PD. Multiplications and mutations of the α-Syn gene (*SNCA*) cause PD-associated syndromes and animal models that overexpress α-Syn replicate several features of PD. Decreasing total α-Syn levels, therefore, is an attractive approach to slow down neurodegeneration in patients with synucleinopathy. We previously performed a genetic screen for modifiers of α-Syn levels and identified CDK14, a kinase of largely unknown function as a regulator of α-Syn. To test the potential therapeutic effects of CDK14 reduction in PD, we ablated Cdk14 in the α-Syn preformed fibrils (PFF)-induced PD mouse model. We found that loss of Cdk14 mitigates the grip strength deficit of PFF-treated mice and ameliorates PFF-induced cortical α-Syn pathology, indicated by reduced numbers of pS129 α-Syn-containing cells. In primary neurons, we found that Cdk14 depletion protects against the propagation of toxic α-Syn species. We further validated these findings on pS129 α-Syn levels in PD patient neurons. Finally, we leveraged the recent discovery of a covalent inhibitor of CDK14 to determine whether this target is pharmacologically tractable *in vitro* and *in vivo*. We found that CDK14 inhibition decreases total and pathologically aggregated α-Syn in human neurons, in PFF-challenged rat neurons and in the brains of α-Syn-humanized mice. In summary, we suggest that CDK14 represents a novel therapeutic target for PD-associated synucleinopathy.

Keywords: α-Synuclein, Parkinson's disease, Cyclin-dependent kinase 14, Neurodegeneration, Therapeutics

55 **INTRODUCTION**

56 Parkinson's disease (PD) is a neurodegenerative disease that affects over 10 million individuals
57 worldwide (1,2). Individuals with PD present with motor symptoms such as bradykinesia, rigidity,
58 shuffling gait, and resting tremor, as well as non-motor symptoms such as constipation, anosmia
59 and sleep disturbances (3–5). Neuropathologically, PD is characterized by the loss of
60 dopaminergic neurons (DaNs) in the *substantia nigra pars compacta* (SN), as well as the
61 accumulation of α-synuclein (α-Syn) containing inclusions, termed Lewy bodies and Lewy
62 neurites (collectively: Lewy pathology) in surviving neurons (6–8). Current treatments address
63 motor deficits, but are less effective on non-motor aspects of the disease and cannot slow down
64 nor halt neurodegeneration in PD (9). Therefore, identifying new 'druggable' targets for PD is
65 clearly warranted. In addition to being abundantly present in Lewy pathology, point mutations and
66 multiplications in the gene encoding α-Syn, *SNCA*, underlie monogenic variants of PD (10,11).
67 Increased levels of *SNCA* mRNA are also observed in laser-captured SN DaNs from PD patients
68 (12), and animal models that overexpress α-Syn replicate several features of PD (13–15). Thus,
69 there is a clear link between increased α-Syn dosage and PD pathogenesis, highlighting the crucial
70 role of α-Syn in the manifestation of PD (16–19).

71 Since α-Syn dosage is linked to PD, decreasing total α-Syn levels may be a feasible
72 approach to mitigate neurodegeneration in PD patients, regardless of whether oligomeric or
73 fibrillar α-Syn is the toxic culprit. *Snca*-knockout (KO) mice are viable and fertile but display mild
74 cognitive impairments, suggesting that a modest amount of cerebral α-Syn is required to
75 accomplish its physiological role in the synapse (20,21). Titration of excessive α-Syn levels in a
76 non-invasive manner would thus be beneficial in treating a chronic neurodegenerative disease like
77 PD. Specifically, an orally available drug capable of mitigating α-Syn toxicity could offer a

78 minimally invasive approach, a feature particularly important in treating a chronic illness. A
79 pooled RNA interference screen investigating 'druggable' modifiers of α-Syn levels identified
80 cyclin-dependent kinase 14 (CDK14, a.k.a. PFTK1; Cdk14 or Pftk1 in mice) as a regulator of α-
81 Syn (22). CDK14 is a brain-expressed protein kinase with a largely unknown biological function
82 (23). Its expression is upregulated in certain cancers, such as esophageal and colorectal cancer, for
83 which it has generated attention as a therapeutic target (24,25). In fact, this has led to the recent
84 development of FMF-04-159-2, a potent, covalent inhibitor of CDK14 (26).

85 Since decreasing CDK14 leads to a mild reduction in endogenous α-Syn levels (22), we
86 hypothesize that genetic and pharmacological inhibition of CDK14 reduces α-Syn pathology and
87 PD-like phenotypes in mice and human cells. To test this hypothesis, we examined the
88 consequence of *Cdk14* reduction on PD-like features in the preformed α-Syn fibrils (PFFs)-
89 induced PD mouse model. We further explored the role of CDK14 in mediating α-Syn spread in
90 primary neurons. We also tested the effect of CRISPR/Cas9-mediated reduction of *CDK14* in
91 human neurons carrying the PD-linked *SNCA* A53T mutation. Lastly, using the covalent CDK14
92 inhibitor, we investigated if pharmacological inhibition of CDK14 is sufficient to decrease α-Syn
93 levels in rodent and human neurons. In summary, we show that decreasing CDK14, both
94 genetically and pharmacologically, reduces α-Syn accumulation, spread, and modifies α-Syn
95 aggregation.

96

97 **MATERIALS AND METHODS**

98 **Mouse strains**

99 *Cdk14*$^{+/-}$ mice were generated by the Gene Targeting and Transgenic Facility of Texas A&M
100 Institute for Genomic Medicine (TIGM), on a mixed (129/SvEvBrd x C57BL/6) background (as

101 described previously (27). *Cdk14*$^{+/-}$ mice were backcrossed 14 times to the C57Bl/6NCrl
102 background prior to experimentation. *Cdk14*$^{+/-}$ mice were paired to generate *Cdk14*$^{-/-}$ mice. *PAC*
103 *α-Syn*^{A53T} *TG* founder mice (dbl-PAC-Tg(*SNCA*^{A53T})$^{+/+}$;*Snca*$^{-/-}$, (28)) were provided by Robert L.
104 Nussbaum (University of California, San Francisco, USA). Mice were genotyped using genomic
105 DNA extracted from ear or tail tissue (genotyping protocol available upon request).
106

107 **Stereotactic PFF injections**

108 Endotoxin-free recombinant mouse α-Syn fibril preparations were stored at -80 ºC before usage
109 (29,30). On the day of the stereotactic injections, fibrils were thawed and sonicated in a sonicator
110 water bath to generate PFFs (Covaris S220, 18 W peak incident power, 20 % duty factor, 50 cycles
111 per burst, 150 seconds). For transmission electron microscopy (TEM) analysis 0.2 mg/mL PFF
112 samples were stained with Uranyl Acetate and imaged on an FEI Tecnai G2 Spirit Twin TEM
113 (Centre for Advanced Materials Research [CAMaR], University of Ottawa). 6-month-old mice
114 were deeply anesthetized with isoflurane, and 1 µL PFFs (5 mg/mL) or sterile saline (0.9 % NaCl)
115 was unilaterally delivered into the dorsal striatum of the right hemisphere at these coordinates
116 relative to bregma: -2 mm medial-lateral; +0.2 mm antero-posterior and -2.6 mm dorso-ventral.
117 Injections were performed using a 2 µL syringe (Hamilton Company, Reno, NV, USA) at a rate
118 of 0.1 µL/minute (min) with the needle left in place for at least 3 min before its slow withdrawal.
119 After surgery, animals were monitored, and post-surgical care was provided. Behavioral
120 experiments were performed 6 months post-injection, followed by the collection of the brains at 7
121 months post-injection.
122

123 **Intracerebroventricular administration of the CDK14 inhibitor FMF-04-159-2**

124 Alzet® Mini-Osmotic Pumps (model 2004) were loaded with FMF-04-159-216 (R&D Systems
125 7158, Minneapolis, MN, USA) 1.47 µg/uL in vehicle solution containing 8 % DMSO (Fisher
126 Scientific, BP231, Hampton, NH, USA), 2 % Tween 80 (Fisher Scientific, BP338-500) and 90 %
127 ddH_2O) 16 hours before stereotactic surgeries. Brain infusion catheters with 3.5 cm long catheter
128 tubing (Alzet® Brain Infusion Kit) were attached as per manufacturer's instructions. Brain
129 infusion assemblies were incubated at 37 °C in sterile saline until implantation. 4-month-old *PAC*
130 *α-Syn*^{A53T} *TG* were deeply anesthetized with isoflurane for the stereotactic implantation of brain
131 infusion assemblies. FMF-04-159-2 (release rate of 0.35 mg/kg/day) or its vehicle solution was
132 continuously administered into the cerebral ventricles (coordinates relative to bregma: -1.1 mm
133 medial-lateral; -0.5 mm antero-posterior and -3 mm dorso-ventral) for 28 days with the brain
134 infusion catheter attached to the skull and the connected pump in a subcutaneous pocket of the
135 mouse's back. The body weight of mice was measured and their activity, neurological signs, facial
136 grimace, coat condition and respiration were scored (from 0 to 3) within 28 days after the surgery.
137 Mice were sacrificed and organs were collected on the 28th day of the administration period.
138

139 **Behavioral experiments**

140 Grip strength tests were performed by holding the mice at an automatic grip strength meter
141 (Chatillon DFE II, Columbus Instruments, Columbus, OH, USA) allowing them to grip the grid
142 of the device with their fore- and hindlimbs. Then, mice were gently pulled back by their tail until
143 they released the grip. Force exerted by the mouse during its removal from the grid, as measured
144 by gram force (g), was evaluated 5 times per mouse. For nesting behavior tests, mice were singly
145 caged overnight (16 hours) with a 5 cm x 5 cm cotton nestlet in a clean cage. Produced nests were
146 scored on a scale from 1to 5 as previously described (31). For the tail suspension test, the tails of

147 the mice were taped to a metal bar attached to the ENV-505TS Load Cell Amplifier and DIG-735
148 cabinet with high pass filter set to 1 Hz (Med Associates, Fairfax, VT, USA). The time of
149 immobility was tested over 6 min. For the elevated plus maze test, mice were placed in the center
150 of a maze consisting of two arms (6 cm x 75 cm), one open and the other enclosed. Over 10 min,
151 the number of open arm entries was tracked with Ethovision software (Noldus Information
152 Technology, Leesburg, VA, USA) and normalized to the total amount of arm entries. For the Y
153 maze test, mice were placed in the center of the Y maze, where the three arms meet and given 8
154 min to explore. The number of arm alternations is measured relative to total arm entries using
155 Ethovision software. For the open field test, mice were placed in a 45 cm x 45 cm open top cage
156 and locomotion was automatically tracked with an overhead-mounted camera connected to a
157 computer equipped with Ethovision tracking software (Noldus Information Technology). Open
158 field motor activity was recorded over 10 min. For the hanging wire test, mice were placed on a
159 wire cage lid which was gently turned upside down over a cage, followed by the recording of the
160 latency to falling from the lid. Mice were given three consecutive training trials, followed by three
161 test trials. The average latency to fall was normalized to the body weight of the mouse. Pole tests
162 were performed by placing the mice on the top of a vertical pole (8 mm diameter and 55 cm height)
163 with a rough surface. Mice were placed vertically, on the top of the pole, and the time required for
164 turning was recorded. The mean time to turn was calculated from 5 consecutive trials for each
165 mouse. For the rotarod test, mice were placed on a rotating, textured rod (IITC Life Science,
166 Woodland Hills, CA, USA), with the speed gradually increasing from 4 to 40 rpm over 5 min. The
167 latency to fall from the rotating rod was recorded for every mouse. Four trials per day with 10 min
168 inter-trial intervals were performed for three consecutive days.
169

170

171 **Tissue harvesting and processing**

172 For biochemical approaches mice were anesthetized with isoflurane (Fresenius Kabi, CP0406V2,
173 Bad Homburg, Germany), and decapitated. Brain tissue of 5-month-old *PAC α-Syn*^{A53T} *TG* mice
174 was weighed and lysed 1:3 (w/v) in PEPI buffer (5 mM EDTA, protease inhibitor [GenDEPOT,
175 P3100, Katy, TX, USA] and phosphatase inhibitor [GenDEPOT, P3200] in PBS) with a Dounce
176 homogenizer. Samples were further lysed 1:6 (w/v) using the tissue weight in TSS Buffer (140
177 mM NaCl, 5 mM Tris–HCl), then TXS Buffer (140 mM NaCl, 5 mM Tris–HCl, 0.5 % Triton X-
178 100), and SDS Buffer (140 mM NaCl, 5 mM Tris–HCl, 1 % SDS), as previously described (32).
179 For immunohistology with paraffin sections, mice were anesthetized with 120 mg/kg Euthanyl
180 (DIN00141704) and intracardially perfused with 10 mL of PBS, followed by 20 mL of 10 %
181 Buffered Formalin Phosphate (Fisher Scientific, SF100-4). Brains were isolated and fixed in 10 %
182 Buffered Formalin Phosphate at 4 °C for at least 24 hours. After dehydration by 70 %, 80 %, 90
183 % and 100 % ethanol and clearing by Xylenes, brains were infiltrated and embedded in paraffin
184 (Louise Pelletier Histology Core Facility, University of Ottawa). Brains were sectioned at 5 µm.

185

186 **SDS-PAGE and mouse protein immunoblots**

187 4X Laemmli buffer (Bio-Rad, 1610747, Hercules, CA, USA) with 20 % 2-mercaptoethanol (Bio-
188 Rad, 1610710) was added to cleared protein and boiled at 95 °C for 5 min. Protein samples were
189 loaded on a 12 % SDS-PAGE gel in the Mini-PROTEAN Tetra Cell (Bio-Rad, 165-8000). Protein
190 was then transferred to a 0.2 µm nitrocellulose membrane (Bio-Rad, 1620112) using the Mini
191 Trans-Blot Electrophoretic Transfer Cell (Bio-Rad, 1703930) in Tris-Glycine buffer with 10 %
192 methanol (Fisher Scientific, A412P) at 340 mA for 90 min at 4 °C. Membranes were then blocked

193 in 5 % milk in 1X TBS-T for 1 hour at room temperature followed by overnight incubation in
194 primary antibody against pSer129 (pS) α-Syn (1:2 000, Abcam, 51253, Cambridge, UK), α-Syn
195 (1:2 000, BD Biosciences, 610787, Franklin Lakes, NJ, USA), CDK14 (1:500, Santa Cruz
196 Biotechnology, sc50475, Dallas, Texas, USA) and GAPDH (1:40 000, Proteintech, 60004-1-Ig,
197 Rosemont, IL, USA) diluted in 2 % BSA, 0.02 % NaN_3 in 1X TBS-T. Next, membranes were
198 washed in TBS-T, followed by incubation in secondary antibody (peroxidase-conjugated donkey
199 anti-rabbit IgG, (Cedarlane, 711-035-152, Burlington, ON, Canada) or donkey anti-mouse IgG,
200 (Cedarlane, 715-035-150), both at 1:10 000 diluted in 5 % milk in TBS-T) for 1 hour at RT.
201 Membranes were washed again in TBS-T, bathed in enhanced chemiluminescent reagent (Bio-
202 Rad, 1705061), imaged using the ImageQuant LAS 4100 Imaging system (GE) and quantified
203 using Image Lab 6.1 software (Bio-Rad).
204

205 **Dopamine Measurements with liquid chromatography-mass spectrometry/mass**
206 **spectrometry (LC-MS/MS)**

207 Striatal tissue punches from 3 mm thick brain sections from 12-month-old PFF-treated mice were
208 weighed and submitted to The Metabolomics Innovation Centre (TMIC, Edmonton, AB, Canada)
209 for analysis. Samples were homogenized in 50 µL of tissue extraction buffer, followed by
210 centrifugation. Dopamine content in µM was analyzed by reverse-phase LC-MS/MS custom assay
211 in combination with an ABSciex 4000 QTrap® tandem mass spectrometer (Applied Biosystems/
212 MDS Analytical Technologies, Foster City, CA, USA) using isotope-labeled internal standards.
213 The assay utilizes a 96 deep well plate with a filter plate attached on top. Samples were thawed on
214 ice, vortexed and centrifugated at 13 000 x g. 10 µL of sample was loaded in the center of the filter
215 and dried in a stream of nitrogen. Following derivatization by phenyl isothiocyanate and drying of

216 filter spots, dopamine content was extracted by adding 300 µL of extraction solvent, centrifugation
217 into the lower collection plate and dilution by MS running solvent. Mass spectrometric analysis
218 was performed with the ABSciex 4000 QTrap® tandem mass spectrometer in combination with
219 an Agilent 1260 series UHPLC system (Agilent Technologies, Palo Alto, CA, USA). Samples
220 were delivered by an LC method followed by a direct injection method. Data was analyzed using
221 Analyst 1.6.2 and expressed as dopamine concentration relative to tissue weight.
222

223 **Histology**

224 For Diaminobenzidine (DAB) antibody staining, paraffin sections were deparaffinized in xylenes
225 and rehydrated in a series of decreasing ethanol (100 %, 90 %, 70 %, 50 %) followed by antigen
226 retrieval in sodium citrate buffer (2.94 g sodium citrate, 0.5 mL Tween 20 in 1 L PBS, pH6) at 80
227 °C for 2 hours and quenching of endogenous peroxidase with 0.9 % H_2O_2 in PBS for 10 min.
228 Sections were blocked in blocking buffer (0.1 % Triton X-100, 10 % normal horse serum in PBS)
229 and incubated in primary antibody (pSer129 α-Syn, 1:500, Abcam, ab51253 or tyrosine
230 hydroxylase, 1:500, Sigma-Aldrich, AB152, St. Louis, MO, USA) overnight at 4 ºC. Then,
231 sections were incubated in secondary antibody (donkey anti-rabbit biotin-conjugated, Jackson
232 ImmunoResearch, 711-065-152, West Grove, PA, USA) 1:125 in blocking buffer for 2 hours and
233 tertiary antibody solution (streptavidin-horseradish peroxidase conjugated, 1:250 in blocking
234 buffer, Sigma-Aldrich, RPN1231V) for 2 hours before being exposed to DAB (Vector
235 Laboratories, SK-4100, Newark, CA, USA) for 10 min. Hematoxylin counterstaining was
236 conducted using the hematoxylin and eosin (H&E) Staining Kit (Abcam, ab245880) as per
237 manufacturer's instructions. Stained sections were dehydrated in a series of ethanol and xylenes

solutions, followed by mounting sections with Permount (Fisher Scientific, SP15-100) and covering with coverslips.

H&E stainings were performed by the Louise Pelletier Histology Core Facility at the University of Ottawa with a Leica Autostainer XL (Leica Biosystems Inc, Concord, ON, Canada). After deparaffinization, sections were exposed to hematoxylin for 7 min and eosin for 30 sec. Then, sections were dehydrated, mounted and covered with coverslips.

For immunofluorescence antibody staining, tissue sections and primary neurons were incubated in primary antibody (Synapsin, 1:2 000, Thermo Fisher Scientific, Waltham, MA, USA, A-6442, PSD95, 1:500, Synaptic Systems, Göttingen, Germany, 124 011, pSer129 α-Syn, 1:500, Abcam, ab51253, Map2, 1:5 000, Abcam, ab5392) in blocking buffer overnight at 4 ºC. Next, sections/neurons were incubated in secondary antibody (goat anti-rabbit IgG (H+L) Alexa Fluor™ 647, Thermo Fisher Scientific, A-21244, for Synapsin, goat anti-mouse IgG (H+L) Alexa Fluor™ 488, Thermo Fisher Scientific, A-11001, for PSD95, goat anti-rabbit IgG (H+L) Alexa Fluor™ 488, Thermo Fisher Scientific, A-11008, for pS129 α-Syn and goat anti-chicken IgY (H+L) Alexa Fluor™ 647, Thermo Fisher Scientific, A-21449, for Map2, all at 1:500) together with DAPI (Sigma-Aldrich, D9542) for 1 hour at RT, followed by mounting sections with fluorescence mounting medium (Agilent, S302380-2). Brightfield and epifluorescence micrographs were acquired using an Axio Scan Z1 Slide Scanner (Carl Zeiss AG, Oberkochen, Baden-Württemberg, Germany) (20x objective, Louise Pelletier Histology Core Facility) and a Zeiss AxioImager M2 (10x objective, Cell Biology and Image Acquisition Core Facility, University of Ottawa) and analyzed using ImageJ (National Institute of Health, Bathesda, MD, USA 1.52p) with 2-3 sections per mouse by a blinded investigator. Heatmaps were generated by counting pS129 α-Syn positive cells in defined regions of the brain (http://atlas.brain-map.org), normalized to the area occupied

261 by the region and resulting cell densities were expressed as hues of red. Micrographs of *in situ*
262 hybridization experiments for the expression of *Snca* (experiment 79908848) and *Cdk14*
263 (experiment 71670684) in the mouse brain were downloaded from the Allen Brain Atlas
264 (http://mouse.brain-map.org/) on August 3rd, 2022.
265
266
267 **Cell culture**
268 Cells were kept at 37 °C, 5 % O_2, 10 % CO_2. For primary mouse cortical neurons coverglass #1.5
269 (Electron Microscopy Sciences, Hatfield, PA) were coated for at least 16 hours at 37 °C, washed
270 twice with ddH_2O and air dried at RT. Mouse embryos at embryonic days 14 to 16 were collected
271 from pregnant females from *Cdk14*$^{+/-}$ crossings (anesthetized with 120 mg/kg Euthanyl). Embryos
272 were decapitated, brains removed, cortices isolated in Hank's Balanced Salt Solution (HBSS)
273 (Millipore Sigma, H9394-500ML) and dissociated in 0.7mg/ml trypsin (Sigma-Aldrich, T4549).
274 Cell suspensions were quickly washed with 150 µg/mL trypsin inhibitor (Roche, Basel,
275 Switzerland, 10109878001) and 666.67 µg/mL DNase 1 (Sigma-Aldrich, DN25-10mg), followed
276 by another wash with 10 µg/mL trypsin inhibitor and 83.34 µg/mL DNase 1 and resuspended in
277 neuronal media (Neurobasal Media (Thermo Fisher Scientific, Gibco 21103049), 1X B27
278 supplement (Gibco, 17504044), 1X N2 supplement (Thermo Fisher Scientific, Gibco 17502-048),
279 1X Penicillin Streptomycin (Thermo Fisher Scientific , Gibco SV30010), and 0.5 mM L-glutamine
280 (Wisent Bio Products, Saint-Jean-Baptiste, QC, Canada, 609-065-EL). Single cells were seeded at
281 ~10^5 cells per coverslip and maintained in culture for 9 (**Fig. S1D** and **S2B**) or 21 days (**Fig. 2**).
282 Neurons were treated with 2 µg/mL of sonicated α-Syn PFFs (StressMarq, Victoria, BC, Canada,
283 SPR-324) at 2 (**Fig. S1D** and **S2B**) or 7 days *in vitro* (DIV) (**Fig. 2**). 14 days after adding PFFs to

284 the neuronal media, media was extracted and passed through a 40 µm cell strainer (VWR, Radnor,
285 PA, USA, 21008-949) for *in vitro* α-Syn spreading experiments (**Fig. 2**). This conditioned media
286 was added to untreated, naïve wildtype (WT) cortical neuron cultures at the time of the media
287 change (7 DIV) and collected for immunofluorescence experiments at 21 DIV. Neurons treated
288 with conditioned media were analyzed by immunofluorescence quantification after 14 days of
289 treatment at 21 DIV. For immunofluorescence staining, cells were fixed in 4 % PFA for 20 min,
290 washed in PBS and incubated in blocking buffer for 1 hour. Cells were incubated with primary
291 antibodies overnight at 4 ºC, followed by incubation with secondary antibodies for 1 hour at RT.
292

293 **hiPSC culture, neuronal differentiation, and Cas9-mediated gene editing**

294 Human induced pluripotent stem cell (hiPSC) isogenic lines (Female) and human embryonic stem
295 cell (hESC) isogenic lines (Male) were generated as described previously (33). hiPSCs were
296 cultured as previously described (34) with slight modifications. Briefly, pluripotent cells were
297 plated in mTeSR (Stem Cell Technologies, Vancouver, BC, Canada) and media was changed daily.
298 The colonies were manually passaged weekly. Differentiation of hPSCs into A9-type DaNs was
299 performed by following a floor plate differentiation paradigm (34,35). Immediately preceding
300 differentiation, the colonies were dissociated into a single cell suspension using HyQTase. hPSCs
301 were collected and re-plated at $4x10^4$ cells/cm^2 on Matrigel (BD Biosciences)-coated tissue culture
302 dishes for differentiation. Floor-plate induction was carried out using hESC-medium containing
303 knockout serum replacement (KSR), LDN193189 (100 nM), SB431542 (10 µM), Sonic Hedgehog
304 (SHH) C25II (100 ng/mL, Purmorphamine (2 µM), Fibroblast growth factor 8 (FGF8; 100 ng/mL),
305 and CHIR99021 (3 µM). On day 5 of differentiation, KSR medium was incrementally shifted to
306 N2 medium (25 %, 50 %, 75 %) every 2 days. On day 11, the medium was changed to

307 Neurobasal/B27/Glutamax supplemented with CHIR. On day 13, CHIR was replaced with Brain
308 Derived Neurotrophic Factor (BDNF; 20 ng/mL), ascorbic acid (0.2 mM), Glial Derived
309 Neurotrophic Factor (GDNF; 20 ng/mL), transforming growth factor beta 3 (TGFβ3; 1 ng/mL),
310 dibutyryl cAMP (dbcAMP; 0.5 mM), and DAPT (10 μM) for 9 days. On day 20, cells were
311 dissociated using HyQTase and re-plated under high cell density $4x10^5$ cells/cm^2 in terminal
312 differentiation medium (NB/B27 + BDNF, ascorbic acid, GDNF, dbcAMP, TGFβ3 and DAPT)
313 also referred to as DA Neuron (DAN)-Medium, on dishes pre-coated with poly-ornithine (15
314 μg/mL)/laminin (1 μg/mL)/fibronectin (2 μg/mL). Cells were differentiated for up to 60 DIV, with
315 analysis being performed at DIV14, DIV 45 and/or DIV 60. At D10D and/or D14D of
316 differentiation, hiPSC cultures were transduced with lentivirus containing Cas9 (lentiCRISPR v2,
317 addgene, plasmid #52961) with the following gRNAs: non-targeting (5'-
318 CGCTTCCGCGGCCCGTTCAA-3'), CDK14 exon 3 (5'-GCAAAGAGTCACCTAAAGTT-3')
319 and exon 8 (5'-TGTGCAAAATATAACGCTGG-3'). From D10D-D14D media was
320 supplemented with 0.1 μM compound E (AlfaAesar, J65131, Haverhill, MA, USA). At D18D,
321 cells were replated onto poly-ornithine (15 μg/mL)/laminin (1 μg/mL)/fibronectin (2 μg/mL)
322 coated plates. Cells were maintained in DAN-medium (DMEM/F12, 200uM Ascorbic Acid, 0.5
323 mM dbcAMP, 20 ng/mL BDNF, 20 ng/mL GDNF, 1 ng/mL TGFb3, and 1 % Anti-Anti) for 6-7
324 weeks where lysates were then collected for protein analysis.
325

326 **hESC culture, neuronal differentiation and *in vitro* CDK14 inhibitor treatment**

327 Neural progenitor cell (NPC) differentiation was performed as previously described (36). Dishes
328 for hESC cultures were coated with 0.15 mg/mL growth factor reduced Matrigel (Corning Inc,
329 354230, Corning, NY, USA) in DMEM/F-12 (Thermo Fisher Scientific, 11320033) for 1 hour at

330 RT prior to cell seeding. H9 hESCs (WiCell, WA09, Madison, WI, USA) were seeded as colonies
331 and maintained in mTeSR Plus (StemCell Technologies, 05825). NPC differentiation was initiated
332 when the hESC cultures reached 90 % confluence, by replacing growth medium with Knockout
333 Serum Replacement (KSR) medium (414 mL Knockout-DMEM (Thermo Fisher Scientific,
334 10829018), 75 mL Knockout-serum replacement (Thermo Fisher Scientific, 10828028), 5 mL
335 Glutamax (Thermo Fisher Scientific, 35050061), 5 mL MEM-NEAA (Thermo Fisher Scientific,
336 11140050), 500 µL 2-mercaptoethanol (Thermo Fisher Scientific, 21985023), 500 µL Gentamicin
337 (Wisent Bioproducts 450-135), 10 µM SB431542 (Tocris, 1614, Bristol, UK) and 500 nM LDN-
338 193189 (Stemgent 04-0074, Reprocell Inc, Yokohama, Kanagawa 222-0033, Japan).
339 Differentiation medium was replaced daily on days 4 and 5 by 75:25 KSR:N2 medium (486.5 mL
340 DMEM/F-12 (Thermo Fisher Scientific, 11320033), 5 mL 15 % glucose, 5 mL N2 supplement
341 (Thermo Fisher Scientific, 17502048), 500 µL 20 mg/mL human insulin (Wisent Bioproducts,
342 511-016-CM), 2.5 mL 1M HEPES (Thermo Fisher Scientific, 15630080), 500 µL Gentamicin),
343 on days 6 and 7 by 50:50 KSR:N2, on days 8 and 9 by 25:75 KSR:N2 and on days 10 and 11 by
344 N2 medium containing 500 nM LDN-193189. On day 12, differentiated NPCs were treated with
345 Y-27632 (Tocris, 1254) for 4 hours, dissociated with Accutase (Stemcell Technologies, 07922)
346 and seeded into Matrigel coated dishes containing Neural Induction Medium (NIM, 244 mL
347 DMEM/F12, 244 mL Neurobasal medium (Thermo Fisher Scientific, 21103049), 2.5 mL N2
348 Supplement, 5 mL B-27 Supplement (Thermo Fisher Scientific, 17504044), 2.5 mL GlutaMAX™
349 (Thermo Fisher Scientific, 35050061), 125 µL 20 mg/mL human insulin, 500 µL 20 µg/mL FGF2
350 (StemBeads, SB500, Rensselaer, NY, USA), 10 µL 1 mg/mL hEGF (Millipore Sigma E9644) and
351 500 µL Gentamicin) for expansion. NPCs were passaged at full confluence a minimum of one
352 time before neuronal differentiation.

353 For NPC-neuronal differentiation culture dishes were coated with 0.001 % Poly-L-ornithine
354 (Millipore Sigma, P4957) at 4 °C overnight, followed by 25 µg/mL laminin (Millipore Sigma,
355 L2020) for 2 hours at room temperature. NPCs were treated with Y-27632 for 4 hours, dissociated
356 with Accutase and seeded at a density of 20 000 cells/cm^2 in NIM. Neuronal differentiation was
357 initiated when NPCs reached 70 % confluence by replacing growth medium with neuronal
358 differentiation medium (244 mL DMEM/F-12 medium, 244 mL Neurobasal medium, 2.5 mL N2
359 supplement, 5 mL B27 supplement, 200 µL 50 µg/ml BDNF (Peprotech, 450-02), 200 µL 50 µg/ml
360 GDNF (Peprotech 450-10, Thermo Fisher Scientific), 250 mg dibutyryl cyclic-AMP (Millipore
361 Sigma, D0627), 500 µL 100 M L-ascorbic acid (FujiFim Wako Chemicals, 323-44822, Osaka,
362 Japan), and 500 µL Gentamicin). Cells were fed every 3 days for 18 days to obtain immature
363 neuronal networks. FMF-04-159-2 was dissolved in DMSO (Fisher Scientific, BP231) and applied
364 in cell culture medium to hESC-derived neurons for 6 days (with a replenishment of FMF-04-159-
365 2 -containing medium after the first 3 days). For protein analysis cells were washed with cold PBS,
366 scraped, and collected in low protein binding microcentrifuge tubes (Thermo Scientific, 90410).
367 Cells were pelleted by centrifugation at 1 000 x g for 5 min at 4 °C. The supernatant was aspirated,
368 and the cells were lysed in cold RIPA buffer (50 mM Tris, pH 7.5, 150 mM NaCl, 0.1 % SDS, 0.5
369 % sodium deoxycholate; 1 % NP-40, 5 mM EDTA, pH 8.0) with protease and phosphatase
370 inhibitors. Cell lysates were incubated on ice for 20 min, with vortexing every 5 min. Lysates were
371 centrifuged at 18 000 x *g* for 20 min at 4 °C to pellet cell debris.
372

373 **ELISA (Enzyme-Linked ImmunoSorbent Assay)**

374 ELISA α-Syn protein quantification was performed as previously described (37,38). 384-well
375 MaxiSorp plates (Nunc, Inc) were coated with capturing antibody (α-Syn, BD Biosciences,

376 610787) diluted 1:500 in coating buffer ($NaHCO_3$ with 0.2 % NaN3, pH9.6) overnight at 4 °C.
377 Following 3 washes with PBS/0.05 % Tween 20 (PBS-T), plates were blocked for 1 hour at 37 °C
378 in blocking buffer (1.125 % fish skin gelatin; PBS-T). After 3 washes, samples were loaded in
379 duplicates and incubated at RT for 2 hours. Biotinylated hSA4 antibody (in-house antibody) was
380 generated using 200 µg Sulfo-NHS-LC Biotin (Pierce, Thermo Fisher Scientific), diluted 1:200 in
381 blocking buffer and added to the plate for 1 hour at 37 °C. Following 5 washes, ExtrAvidin
382 phosphatase (Sigma, E2636) diluted in blocking buffer was applied for 30 min at 37 °C. Color
383 development was carried out by using fast-p-nitrophenyl phosphate (Sigma, N1891) and
384 monitored at 405 nm every 2.5 min for up to 60 min. Saturation kinetics were examined for
385 identification of time point(s) where standards and sample dilutions were in the log phase.
386

387 **Primary rat neurons, human α-Syn PFFs and protein analysis**

388 Cortical neurons were harvested from the E18 Sprague Dawley rat embryos (Charles River,
389 Wilmington, MA, USA). The harvested cortical tissue was digested using 17 U/mg Papain
390 followed by mechanical dissociated by gentle trituration through a glass flamed Pasteur pipet. The
391 cells were seeded into plates coated 24 hours prior to dissection with Poly-D-Lysine (0.15 mg/mL).
392 The cells were incubated at 37 °C, 7.5 % CO_2 until collection. Every 3 to 4 days, a 50 % media
393 change was performed (2 % B27 supplement, 1 % antibiotic/antimycotic, 0.7 % BSA Fraction V,
394 0.1 % β-mercaptoethanol in HEPES-buffered DMEM/F12). Where required, cells were exposed
395 to 100 nM FMF-04-159-2 (Bio-Techne, 7158/10, Minneapolis, MN, USA) dissolved in DMSO,
396 at 14 DIV, and again at the subsequent feed (18 DIV). At 14 DIV, cells were exposed to either 1
397 µg/mL human α-Syn PFFs, or 1 µg/mL monomeric α-Syn. Cell lysates were collected at day 5
398 post PFF or monomeric exposure. Human α-Syn protein was isolated from BL21-CodonPlus

399 (DE3)-RIPL competent cells transformed with pET21a-alpha-synuclein and purified by Reversed-
400 phase HPLC. PFFs were then generated as previously described (39). Purified α-Syn (5 μg/mL in
401 PBS) was incubated at 37 °C with constant shaking for 7 days, then aliquot and stored at -80 °C.
402 Prior to use, PFFs were thawed and diluted in PBS, then subjected to sonication (20% amplitude,
403 30 seconds; 1 second on, 1 second off) and added to neuronal media for exposure to neurons at a
404 concentration of 1 μg/mL for 24 hours. Following the incubation, cell lysates were collected in
405 150 μL ice-cold RIPA buffer containing phosphatase and protease inhibitors (1 mM aprotinin, 1
406 mM sodium orthovanadate, 1 nM sodium fluoride, and 10 mM phenylmethylsulfonyl fluoride).
407 Samples were homogenized using an 18G needle, left on ice to rest for 15 min, and then
408 centrifuged at 14 000 *g* to remove any cellular debris. For the soluble fraction, cells were lysed in
409 1 % Tx-100 in TBS buffer (TXS buffer) and cleared by ultracentrifugation at 100 000g for 30 min.
410 Pellets were washed twice with 1 % Tx-100 in TBS, then resuspended in 8M Urea + 8 % SDS in
411 TBS buffer (Urea buffer) to generate the insoluble fraction. Using the BioRad DC Protein Assay
412 kit, the protein concentration of each sample was quantified following the manufacturer's
413 guidelines. SDS-PAGE was performed using 12.5 % resolving gels and 4 % stacking gels, and
414 gels were run for 15 min at 80 V followed by approximately 1.5 hours at 110 V. The gels were
415 transferred onto 0.2 μM nitrocellulose membranes at 35 V and 4 °C overnight. Following the
416 transfer, the membranes were blocked for 1 hour at room temperature using blocking buffer (5 %
417 non-fat dry milk in 1 X TBST) with constant agitation. Primary antibodies were prepared in
418 blocking buffer containing 0.1 % Tween 20 and were probed overnight at 4 °C under constant
419 agitation (CDK14, 1:1 000, Santa Cruz Biotechnology, sc50475; TH, 1:1 000, Pel Freeze
420 Biologicals, Rogers, AR, USA, P40101; a-Syn, 1:1 000, BD Biosciences, 610787; pS129 a-Syn,
421 1:500, abcam, ab51253; β-Actin, 1:1 000, rabbit, Biolegend, San Diego, CA, USA, 622101 or

422 mouse, Sigma, A5411, βIII-Tubulin, 1:5 000, rabbit, Biolegend, 802001). Following primary
423 antibody incubation, membranes were rinsed using 1XPBS containing 0.1 % Tween 20 and
424 subsequently re-blocked using the blocking buffer. The membranes were then probed with
425 secondary antibody for 1 hour at RT in blocking buffer containing 0.1 % Tween 20 (Goat anti-
426 Mouse IgG (H+L) Secondary Antibody, HRP (Thermo Fisher Scientific, 31430); Goat anti-Rabbit
427 IgG (H+L) Secondary Antibody, HRP (Thermo Fisher Scientific, 31460); Li-Cor infrared
428 conjugated secondary/ IRDye 800RD Donkey anti-Rabbit IgG antibody (LI-COR Biosciences,
429 926-32211, Lincoln, NE, USA) at dilutions of 1:2 000). The membranes were rinsed to remove
430 any residual blocking buffer using 1X PBS containing 0.1 % Tween 20. If HRP-conjugated
431 secondary antibodies were used, membranes were probed for 5 minutes with clarity Western
432 enhanced chemiluminescence blotting substrate (Bio-Rad) and visualized with photosensitive
433 film. For LiCOR-secondary antibodies, membranes were visualized with a LiCOR Odyssey Fc.
434 Total protein was visualized by Coomassie Brilliant Blue (0.1 % Coomassie, 50 % Methanol and
435 10 % glacial acetic acid in ddH_2O).
436

437 **Statistics**

438 Statistical analysis was performed using GraphPad Prism version 9.2.0. Quantified data are
439 visualized as mean + standard error of the mean (SEM). Unpaired student's *t* tests were used for
440 two-group comparisons. Data affected by one or two factors were analyzed by one-way or two-
441 way analysis of variance (ANOVA), respectively, followed by Bonferroni *post hoc* comparisons
442 (unless otherwise stated in the figure legend) when at least one of the main factors or the interaction
443 was significant. A significance level of 0.05 was accepted for all tests. Asterisks mark P values ≤
444 0.05 (*), ≤ 0.01 (**), ≤ 0.001 (***), or ≤ 0.001 (****).

445

446 **RESULTS**

447 **CDK14 ablation limits grip strength deficits and reduces cortical α-Syn pathology in PFF-**
448 **injected mice**

449 We first examined existing *in situ* hybridization data for the expression of *Snca* and *Cdk14* in the
450 murine brain. We observed that both genes are expressed in similar brain regions, including the
451 hippocampus and the SN (**Fig. S1A**). Since PD is a chronic disease, inhibition of a candidate
452 modifier would have to be safe in the long term. We analyzed Cdk14 protein levels in different
453 mouse organs and tested the effects of Cdk14 depletion on survival, fertility, and organ
454 cytoarchitecture *in vivo*. We found that CDK14 protein is highly abundant in the brain, as well as
455 in the lung and the spleen (**Fig. S1B**). Cdk14 nullizygous mice are viable, fertile, and exhibited
456 normal brain morphology (**Fig. S1C**, (27)) and synaptic integrity (**Fig. S1D**). Furthermore, we did
457 not observe altered morphology of the lung and spleen by Cdk14 ablation (**Fig. S1E**). We next
458 asked whether silencing *Cdk14* is sufficient to mitigate behavioral and histological phenotypes
459 observed in cultured neurons and in mice exposed to pathogenic α-Syn pre-formed fibrils (mouse
460 PFFs; **Fig. 1A** and **B**; **Fig. S2A**). 6 months following intrastriatal injection of α-Syn PFFs, there is
461 a stereotypic brain-wide accumulation of pS129 α-Syn – a marker of human synucleinopathies –
462 in addition to SN DaNs loss and mild motor impairments (40–42). In our experimental paradigm,
463 6 months after PFF injection (at an age of 12 months), we found that PFF injected WT mice
464 exhibited reduced forelimb force generation in the grip strength test compared to their saline-
465 treated counterparts (**Fig. 1B**), similar to what has been previously reported (41,42). In contrast,
466 the PFF-induced weakening of grip strength was not observed in *Cdk14*$^{+/-}$ or in *Cdk14*$^{-/-}$ mice. We
467 did not observe PFF-mediated changes (in any genotype tested) in the other 8 behavioral tests

468 conducted (including tests for cognitive and motor function). Importantly, we noted that saline-
469 injected *Cdk14*$^{+/-}$ and *Cdk14*$^{-/-}$ mice consistently performed like their WT counterparts in each test,
470 suggesting that chronic Cdk14 reduction is not deleterious to the brain (**Fig. S2C**).
471 Next, we analyzed the relative pathological burden of accumulated α-Syn throughout the brain of
472 mice injected with PFFs. We stained for synucleinopathy-linked pS129
473 α-Syn in the brain of WT mice and found high amounts of pS129 α-Syn-positive cells in the PFF-
474 injected hemisphere (ipsilateral to the injection, IL), which were absent in saline-injected controls
475 (data not shown). We then mapped the distribution of α-Syn pathology at three different
476 rostrocaudal levels near the injection site (relative to bregma: +0.98 mm, +0.26 mm and -1.34 mm)
477 and found an overall blunting of pS129 α-Syn-positive pathology in the PFF-injected *Cdk14*$^{+/-}$ and
478 *Cdk14*$^{-/-}$ mice compared to their WT littermates (**Fig. 1C**). This was particularly evident at
479 anatomical regions distal from the injection site, such as the somatomotor cortex (bregma +0.26
480 mm) and in other cortical areas. Surprisingly, α-Syn pathology proximal to the injection site in the
481 striatum was not significantly affected between PFF-injected genotypes (**Fig. 1C**). Similarly to
482 cortical regions of PFF-injected *Cdk14*$^{-/-}$ mice, we observed fewer pS129 α-Syn-positive neurons
483 in *Cdk14*$^{-/-}$ mouse primary cortical cultures treated with PFFs compared to their WT littermate
484 controls (**Fig. S2B**).
485 Previous reports have shown that α-Syn PFFs can induce nigrostriatal degeneration over time
486 (40–42). We stained for tyrosine hydroxylase (TH) at the injection site in the striatum and observed
487 a similar decrease of TH-positive dopamine fibers in WT, *Cdk14*$^{+/-}$ and *Cdk14*$^{-/-}$ mice injected with
488 PFFs ipsilateral to the injection, relative to their saline-treated counterparts (**Fig. 1D**). PFF-induced
489 loss of dopamine fibers was not accompanied by altered striatal dopamine content (**Fig. S2D**). TH
490 staining in the midbrain revealed equal loss of SN DaNs in PFF-injected WT, *Cdk14*$^{+/-}$ and

491 *Cdk14*$^{-/-}$ mice in comparison to saline-injected controls (**Fig. S2D**). Together, these data show that
492 loss of Cdk14 blunts cortical α-Syn histopathology and PFF-induced grip strength impairment
493 without evidently halting nigrostriatal neurodegeneration in the PFF model. It was interesting to
494 note that the effect of Cdk14 on α-Syn was selective to pathological forms of the protein, as partial
495 reduction or ablation of Cdk14 in *Cdk14*$^{+/-}$ or *Cdk14*$^{-/-}$ mice, respectively, did not change levels of
496 endogenous mouse α-Syn (**Fig. S2E**).
497

498 **Cdk14 loss decreases α-Syn cell-to-cell spread in cortical neuron culture**

499 Our *in vivo* data suggest that decreasing Cdk14 reduces distal (e.g. contralateral; higher cortical
500 area) pathology, while not affecting pathology close to the injection site. We hypothesized that
501 Cdk14 may preferentially affect the cell-to-cell spread of α-Syn, thus contributing to this
502 phenomenon. To test this, we cultured primary neurons of WT, *Cdk14*$^{+/-}$ and
503 *Cdk14*$^{-/-}$ embryos, treated them with mouse PFFs at 7 days in culture and collected media 14 days
504 post PFF application (a time where most of the exogenous fibrils have been depleted from the
505 system ((43); schematic in **Fig. 2A**). We applied this filtered, seed-competent media to naïve WT
506 cultures to test the seeding capacity of α-Syn and found that loss of Cdk14 dramatically reduced
507 α-Syn pathology (measured by pS129 α-Syn accumulation), 14 days following media application
508 (**Fig. 2B**).
509

510 **Knockdown of CDK14 decreases pS129 α-Syn levels in human neurons**

511 Having observed the benefits of Cdk14 depletion in the PFF mouse model of PD, we next tested
512 whether this benefit translates to human neurons. We infected DaNs derived from a PD patient
513 carrying an A53T mutation in α-Syn (33) as well as its isogenic control with lentiviruses carrying

514 Cas9/sgRNAs against *CDK14*. Neurons infected with sgRNAs targeting either exon 3 (E3) or exon
515 8 (E8) of *CDK14*, exhibited approximately 50 % of the CDK14 levels of the control cultures (**Fig.**
516 **3**). We found that A53T mutant cells show a marked increase of pS129 α-Syn compared to isogenic
517 controls, and that *CDK14* knockdown significantly lowers pS129 α-Syn levels (**Fig. 3**).
518

519 **Pharmacological targeting of CDK14 decreases α-Syn levels and mitigates its pathogenic**
520 **accumulation**

521 As kinases are typically druggable targets which can be inhibited in non-invasive ways (44), we
522 next asked whether CDK14 inhibition would be a tractable route for decreasing α-Syn levels. We
523 used a recently developed CDK14 covalent inhibitor (FMF-04-159-2) (26) to test whether acute
524 inhibition of CDK14 reduces α-Syn levels. We treated hESC-derived cortical neurons with the
525 CDK14 inhibitor for 6 days and observed a dose-dependent reduction in total α-Syn concentration
526 by ELISA (**Fig. 4A**). We also tested whether the CDK14 inhibitor affects the α-Syn load in rat
527 primary neuronal cultures treated with α-Syn PFFs. Here, PFF treatment induced a spike in
528 insoluble (Urea buffer-soluble) α-Syn protein, which CDK14 inhibition markedly reduced (**Fig.**
529 **4B**). Interestingly, the PFF treatment also induced an increase of CDK14 insoluble protein, which
530 was not present in untreated neurons or in neurons treated with α-Syn monomers (**Fig. 4B**).
531

532 ***In vivo* inhibition of CDK14 decreases the load of human α-Syn**

533 Since the treatment of human neurons and PFF-challenged rat neurons with the CDK14 inhibitor
534 showed a reduction in total and insoluble α-Syn protein, respectively, we next tested whether
535 pharmacological inhibition of CDK14 modifies α-Syn levels *in vivo*. We administered FMF-04-
536 159-2 via intracerebroventricular infusion at 0.35 mg/kg/day for 28 days in 4-month-old *PAC α-*

537 *Syn*^{A53T} *TG* mice (**Fig. 5A**) which harbor the PD-associated A53T mutant human α-Syn gene in
538 the absence of mouse *Snca* (28). Administration of the CDK14 inhibitor did not modify body
539 weight development, nor induce any signs of distress or pain as indicated by alterations of
540 locomotion, facial expression, or coat condition of *PAC α-Syn*^{A53T} *TG* mice in comparison to
541 vehicle-treated counterparts (**Fig. S3A**). Similarly, CDK14 inhibitor treatment did not induce
542 changes in the cytoarchitecture of the lung, spleen, and liver (**Fig. S3B**). To quantify levels of
543 pathogenic forms α-Syn, we collected brains after 1 month of CDK14 inhibitor treatment (**Fig.**
544 **5A**) and analyzed protein content of the TSS, TXS and SDS buffer-soluble fractions (**Fig. 5B**). We
545 observed a reduction of total α-Syn and low molecular weight α-Syn species, suggestive of
546 decreased C-terminally truncated (CTT) α-Syn in CDK14 inhibitor-treated mice relative to their
547 vehicle controls. Interestingly, levels of pS129 α-Syn were increased in CDK14 inhibitor treated
548 mice in the TSS buffer-soluble fraction, whereas it was decreased in the TXS buffer-soluble
549 fraction. Notably, CDK14 levels were specifically decreased (target engagement) in the TXS and
550 SDS buffer-soluble fractions, but not the TSS buffer-soluble fraction, of inhibitor-treated mice.
551 Together these results show that *in vivo* administration of the CDK14 inhibitor in the brain engages
552 its target and mitigates certain pathogenic forms of human α-Syn in the mouse brain in a protein
553 fraction-dependent manner without inducing obvious discomfort or pain.
554

555 **DISCUSSION**

556 α-Syn is increasingly considered a valid experimental therapeutic target for PD, based on clinical
557 genetic and neuropathological evidence, as well as animal and cell culture studies. *SNCA* gene
558 mutations or amplifications resulting in α-Syn pathology are tightly linked to PD pathogenesis.
559 Moreover, α-Syn is a major constituent of Lewy-like structures, the pathological hallmark of PD

560 and related synucleinopathies. Thus, targeting α-Syn has been a major thrust in the pharmaceutical
561 realm. One aspect of α-Syn pathology that has been difficult to overcome is the notion that different
562 states of its post-translational modification or aggregation differentially affect disease
563 pathogenesis: a clear image has yet to emerge as to the real culprit of α-Syn toxicity. Although
564 novel strategies such as anti-sense oligonucleotides, immunotherapy and small molecule inhibitors
565 of α-Syn aggregation are being explored (45), finding a target that can be pharmacologically
566 inhibited still holds potential as a minimally invasive and simple strategy to lower α-Syn levels –
567 especially when such treatment course would be made over several decades. Indeed, a growing
568 body of evidence suggests that α-Syn may play a role not only at the presynaptic space but also in
569 the immune system (37,46,47). Therefore, careful titration of its levels may be clinically crucial.
570 As a result, we asked whether candidates that are more amenable to traditional pharmacology (i.e.
571 kinases) could regulate α-Syn dosage, irrespective of its aggregation status. Our previous studies
572 identified a handful of these modifiers including TRIM28 and DCLK1 (8,22,48,49). Here, we
573 study a heretofore unexplored target as well as its newly developed cognate inhibitor (26) for
574 disease modification in pre-clinical models of PD: CDK14.

575 We show that the reduction of CDK14 protein levels is well tolerated and causes a reduction
576 in pathogenic α-Syn accumulation in murine and human models of synucleinopathy. Genetic
577 suppression of *Cdk14* reduces pS129 α-Syn pathology in the cortex of PFF-injected mice and
578 dampens the development of grip strength deficits in these mice; while this rescue is not found at
579 sites proximal to the injection, including the nigrostriatal tract. Importantly, the genetic reduction
580 of CDK14 in DaNs derived from an individual with synucleinopathy shows equal promise in
581 preventing phenotypic development. We show that the selective covalent CDK14 inhibitor, FMF-
582 04-159-2, decreases α-Syn levels in hESC-derived human neurons and mitigates PFF-induced α-

583 Syn pathology in rat cortical neurons. Lastly, we demonstrate that administering FMF-04-159-2
584 *in vivo* reduces α-Syn dosage and, consequently, decreases pathogenic forms of α-Syn in a
585 humanized mouse line expressing PD-linked A53T *SNCA*. Collectively, these results show that
586 CDK14 is a pharmacologically tractable target for synucleinopathy.

587 We observed that loss of Cdk14 in PFF-treated mice reduced the level of α-Syn
588 histopathology in cortical areas, such as the somatomotor cortex. Surprisingly, we did not detect
589 changes in the load of pS129 α-Syn-positive cells by *Cdk14* ablation in the striatum, the PFF
590 injection site (**Fig. 1C**). In line with this, we noticed a similar PFF-induced degeneration of the
591 dopaminergic nigrostriatal system in WT, *Cdk14*$^{+/-}$ and *Cdk14*$^{-/-}$ mice (**Fig. 1D** and **Fig. S2D**).
592 These observations imply that loss of CDK14 reduces the degree of intercellular α-Syn spreading
593 rather than protecting neurons which are directly exposed to PFFs. Indeed, when we tested this in
594 a cultured neuron system, we found that genetic reduction of Cdk14 dramatically decreased the
595 spreading capacity of seed-competent α-Syn (**Fig. 2**). Therefore, it is plausible that CDK14
596 facilitates the cell-to-cell spread of α-Syn. Genetic reduction of CDK14 using a CRISPR/Cas9-
597 mediated strategy in stem cell-derived human neurons carrying the PD-linked *SNCA* A53T
598 mutation lowered levels of pS129 α-Syn (**Fig. 3**), indicating that ablation of both, murine and
599 human *Cdk14*/*CDK14* mitigates the neuronal load of this pathology-linked form of α-Syn.

600 Given the lack of phenotypes in the *Cdk14*$^{-/-}$ or *Cdk14*$^{+/-}$ mice, no evidence for loss of
601 function intolerance in humans (probability of loss of function intolerance [pLI] = 0; gnomAD
602 database, *CDK14* | gnomAD v2.1.1), (50)) and the availability of a recently developed highly
603 selective CDK14 inhibitor, we further explored the pharmacological tractability of CDK14 in the
604 context of synucleinopathy. Treatment of hESC-derived cortical neurons with the newly developed
605 CDK14 inhibitor FMF-04-159-2 induced a pronounced reduction of the total α-Syn concentration,

606 as measured by ELISA quantification (**Fig. 4A)**. FMF-04-159-2 was recently designed to provide
607 an improved pharmacological tool for the inhibition of CDK14 as treatment for colorectal cancer
608 (26). Interestingly, FMF-04-159-2 was described to covalently bind and inhibit CDK14 at ~100
609 nM (IC_{50} = 86 nM (26)), a dosage which lowered α-Syn levels to ~12 % of vehicle-treated controls
610 in our *in vitro* experiments. Applying the CDK14 inhibitor to PFF-challenged rat cortical neurons
611 reduced the amount of aggregated (Urea buffer-soluble) α-Syn species (**Fig. 4B**), phenocopying
612 the low degree of pS129 pathology in cortical neurons of PFF-treated *Cdk14*$^{-/-}$ mice (**Fig. 1C**) or
613 cultures (**Fig. 2** and **Fig. S2B**). Interestingly, we found that Cdk14 accumulated in the urea-soluble
614 fraction, specifically upon PFF treatment. To our knowledge, it is not known whether CDK14 is
615 present in LBs or LNs in brains of PD patients. Future histopathology experiments may generate
616 deeper insights on if CDK14 aggregates together with α-Syn in patients with synucleinopathies.
617 Comparable to CDK14 inhibitor-treated rat neurons with PFFs, we observed a reduction of total
618 α-Syn in the more insoluble, TXS buffer-soluble protein fraction (and in the TSS buffer-soluble
619 fraction) of *PAC α-Syn*^{A53T} *TG* mice which received FMF-04-159-2 via intracerebral injection
620 (**Fig. 5A** and **B**). Reduction of total α-Syn was accompanied by lower amounts of CTT α-Syn,
621 indicating that this form of α-Syn, which increases α-Syn's propensity to aggregate and enhances
622 its cytotoxic effects (51–53), is modulated by CDK14. Levels of pS129 α-Syn were reduced in the
623 more insoluble TXS fraction of CDK14 inhibitor-treated mice, again pointing towards lower
624 degrees of aggregated, pathology-relevant forms of α-Syn. In contrast to these findings, we found
625 paradoxically increased amounts of pS129 α-Syn in the TSS buffer-soluble fraction (highly
626 soluble) of CDK14 inhibitor-treated mice, suggesting that Cdk14 blockage increased pS129 α-Syn
627 in the cytosol of this α-Syn-humanized mouse line. Notably, we did not observe any macroscopic
628 signs of PD/neuropathy-linked behavioral abnormalities in *PAC α-Syn*^{A53T} *TG* mice upon CDK14

629 inhibitor treatment, such as loss of motor activity or imbalance during locomotion (**Fig. S3A**),
630 implying that higher amounts of cytosolic pS129 α-Syn do not substantially promote cerebral and
631 functional impairments. Elevated levels of cytosolic, non-aggregated pS129 α-Syn seem to be
632 indicative of earlier stages of synucleinopathies, as cytoplasmic networks positive for pS129 α-
633 Syn are more commonly observed in neurons without LBs from patients with early-stage disease,
634 than in LB-containing neurons of patients with advanced PD (54). Based on these *in vivo* CDK14
635 inhibitor administration experiments, we hypothesize that blockage of CDK14 activity reduces
636 loads of pathology-linked forms of insoluble α-Syn, potentially shifting synucleinopathy
637 progression to an earlier phase of disease development.

638 Our experiments provide insights in the modulatory effects on α-Syn pathology by reduced
639 CDK14 activity in neurons from multiple mammalian species. However, we did not observe any
640 direct interaction between both proteins, CDK14 and α-Syn. Moreover, we could not detect any
641 kinase activity of recombinant CDK14 toward wild-type α-Syn *in vitro* (data not shown). We
642 therefore hypothesize that loss or inhibition of CDK14 causes a decrease in α-Syn through
643 unknown mediators, ultimately regulating α-Syn protein levels and intercellular spreading of α-
644 Syn pathology. Future studies will help refine the mechanism whereby CDK14 regulates α-Syn.

645 Our results examining the genetic and pharmacological reduction of CDK14 in PD models
646 set the stage for future pre-clinical studies. In all behavioral experiments conducted, *Cdk14*$^{-/-}$ mice
647 were indistinguishable from WT mice (**Fig. 1B** and **Fig. S2C**). Furthermore, loss of Cdk14 did not
648 alter the architecture of brain tissue or peripheral organs (**Fig. S1C** to **Fig. S1E**) implying that
649 *Cdk14* loss is not deleterious *in vivo*. This is supported by human genetics where the loss of *CDK14*
650 appears to be well tolerated. Additionally, Cdk14 inhibition *in vivo* did not induce any signs of
651 discomfort (**Fig. S3A**), implying that pharmacological targeting of CDK14 is safe. Similarly,

652 systemic administration of FMF-04-159-2 at a ~140-fold higher delivery rate (50 mg/kg/day)
653 appears to be well tolerated by mice as shown in a recent study (55) where Cdk14 inhibition
654 mitigated the growth of lung tumors. In our study, the activity of the CDK14 inhibitor in human
655 neurons appears to be high, affecting CDK14 (and thus α-Syn metabolism) in the nanomolar range
656 (**Fig 4A**). Further preclinical experiments will test whether the drug rescues PD-like neuron loss
657 and behavioral phenotypes in models of synucleinopathies; potentially paving the way for its use
658 in humans.

659 In sum, we show that CDK14 inhibition causes a decrease of total α-Syn concentrations
660 under both *ex vivo* and *in vivo* conditions, ameliorates the levels of pathology-relevant forms of α-
661 Syn and potentially reduces cell-to-cell transmission of α-Syn. Given the strong evidence linking
662 α-Syn levels to PD pathogenesis, we conclude that targeting CDK14 function holds promise as a
663 potentially disease-modifying approach to treat PD.

664

665 **CONCLUSIONS**

666 Elevated α-Syn levels are closely linked to PD. In this study, we explore the effect of inhibiting
667 CDK14 as a pharmacologically tractable approach to decrease α-Syn levels in cultured neurons
668 and animal models. We show that the genetic reduction of Cdk14 mitigates grip strength
669 impairment and ameliorates cortical α-Syn pathology in PFF-treated mice, without affecting
670 nigrostriatal pathology proximal to the injection site; Cdk14 likely acts to regulate the intercellular
671 spread of seed-competent α-Syn. Similarly, *CDK14* ablation reduces α-Syn pathology in human
672 dopaminergic neurons derived from PD patients. Finally, pharmacological targeting of CDK14
673 lowers pathological α-Syn in cultured neurons and modifies pathogenic forms of α-Syn in mice

674 expressing PD-linked human A53T *SNCA*. Taken together, we propose CDK14 inhibition as a
675 novel pre-clinical strategy to treat synucleinopathy.
676
677 **LIST OF ABBREVIATIONS**
678 α-Syn: α-Synuclein; BDW: bodyweight; CDK14: cyclin-dependent kinase 14; CL: contralateral;
679 CTT: C-terminally truncated α-Syn; DAB: diaminobenzidine; DaNs: dopaminergic neurons; DIV:
680 days *in vitro*; ELISA: enzyme-linked immunosorbent essay; H&E: hematoxylin and eosin; hESC:
681 human embryonic stem cell; high exp.: high exposure; hiPSC: human induced pluripotent stem
682 cell; IL: ipsilateral; min: minutes; KO: knockout; LC-MS/MS: liquid chromatography – mass
683 spectrometry/mass spectrometry; Mono: α-Synuclein monomers; NPC: neural precursor cell; PBS:
684 phosphate-buffered saline; PD: Parkinson's disease; PFFs: α-Synuclein preformed fibrils; RT:
685 room temperature; sec: seconds; SEM: standard error of the mean; SN: *substantia nigra pars*
686 *compacta*; TG: transgene; UT: untreated; WT: Wildtype
687
688 **DECLARATIONS**
689
690 **Ethics approval and consent to participate**
691 Animal experiments were done under the approved breeding and behavior protocols approved by
692 the University of Ottawa Animal Care Committee. Studies with hESCs were performed following
693 approval by the Stem Cell Oversight Committee of Canada and the Institutional Review Board
694 (Ottawa Health Science Network Research Ethics Board).
695
696 **Consent for publication**

697 Not applicable

698

699 **Availability of data and material**

700 All data of this study are in the main text or in the Supplementary Materials.
701 Cdk14$^{-/-}$ mice were obtained from David S. Park from the University of Calgary and are on an F14
702 C57BL/6N background. *PAC α-Syn*^{A53T} *TG* mice (dbl-PAC-Tg(*SNCA*^{A53T})$^{+/+}$;*Snca*$^{-/-}$, (28)) were
703 provided by Robert L. Nussbaum from the University of California, San Francisco. Any other
704 materials are commercially available.

705

706 **Competing interests**

707 The authors declare that they have no competing interests.

708

709 **Funding**

710 Parkinson's Foundation-APDA Summer Student Fellowship PF-APDA-SFW-1919, Parkinson
711 Research Consortium (PRC) Summer Studentship, University of Ottawa Faculty of Medicine,
712 Office of Francophones Affairs Scholarship, Undergraduate Research Scholarship (URS),
713 University of Ottawa. (JLAP)
714 Parkinson Research Consortium (PRC) Larry Haffner Fellowship, Parkinson Canada Basic
715 Research Fellowship BRF-2021-0000000048. (KMR)
716 Parkinson's Research Consortium (PRC) Bonnie and Don Poole Fellowship, Ontario Graduate
717 Scholarship, Queen Elizabeth II Scholarship. (HMG)
718 Canadian Institutes of Health Research (FRN-153188). (WLS)
719 Vanier Canada. (MGS)
720 Parkinson's Society of Southwestern Ontario (PSSO). (BBD)
721 Canadian Institutes of Health Research (FRN-159443). (SDR)
722 Parkinson's Foundation Stanley Fahn Junior Faculty Award (PF-JFA-1762), Canadian Institutes
723 of Health Research (PJT-169097), the Parkinson Canada New Investigator Award (2018-00016),
724 Aligning Science Across Parkinson's (ASAP-020625) through the Michael J. Fox Foundation for
725 Parkinson's Research (MJFF). (MWCR)
726

727 **Authors' contributions**

Conceptualization: JLAP, KMR, MWCR
Methodology: JLAP, KMR, MS, BBD, EL, BN, NAL, HMG, AB, MGS, BBD, SMC, MWCR
Investigation: JLAP, KMR, MS, BBD, HMG, SMC, MWCR
Supervision: WLS, MGS, SDR, MWCR
Writing – original draft: JLAP, KMR, MWCR
Writing – review & editing: JLAP, KMR, JJT, MGS, WLS, PB, SDR, MWCR
Resources: AJ, JM, PB

Acknowledgements

The authors thank Drs. Eliezer Masliah (UCSD/NIA), Robert L. Nussbaum (UCSF), and David Park (University of Calgary) for sharing the genetically modified mice used in this study. We thank Dr. G. Vázquez-Vélez (Washington University) for his critical appraisal of the manuscript. The authors also thank the following Core facilities from the University of Ottawa and the Ottawa Hospital Research Institute for use of their facility, equipment, and expertise: Animal Behaviour and Physiology Core (RRID: SCR_022882), Cell Biology and Imaging Acquisition Core (RRID: SCR_021845), StemCore Laboratories (RRID: SCR_012601) and Louise Pelletier Histology Core (RRID: SCR_021737). The authors also thank The Metabolomics Innovation Centre (TMIC) for the analysis of the striatal dopamine content and Anthony Carter (Surgical Core Service, University of Ottawa) for his support in stereotactic surgeries. Schemes were generated using biorender (https://biorender.com/).

References and Notes

1. Selvaraj S, Piramanayagam S. Impact of gene mutation in the development of Parkinson's disease. Genes Dis. 2019;6(2):120–8.
2. Mhyre TR, Boyd JT, Hamill RW, Maguire-Zeiss KA. Parkinson's disease. Subcell Biochem. 2012;65:389–455.
3. Sveinbjornsdottir S. The clinical symptoms of Parkinson's disease. J Neurochem. 2016;139:318–24.
4. Mazzoni P, Shabbott B, Cortés JC. Motor control abnormalities in Parkinson's disease. Cold Spring Harb Perspect Med. 2012;2(6):1–17.

5. Berardelli A, Rothwell JC, Thompson PD, Hallett M. Pathophysiology of bradykinesia in Parkinson's disease. Brain. 2001 Nov;124(11):2131–46.
6. Mor DE, Ischiropoulos H. The Convergence of Dopamine and α-Synuclein: Implications for Parkinson's Disease. J Exp Neurosci. 2018 Mar;12:1179069518761360.
7. Fujiwara H, Hasegawa M, Dohmae N, Kawashima A, Masliah E, Goldberg MS, et al. α-Synuclein is phosphorylated in synucleinopathy lesions. Nat Cell Biol. 2002;4(2):160–4. Available from: https://doi.org/10.1038/ncb748
8. Vázquez-Vélez GE, Gonzales KA, Revelli J-P, Adamski CJ, Alavi Naini F, Bajić A, et al. Doublecortin-like Kinase 1 Regulates α-Synuclein Levels and Toxicity. J Neurosci. 2020;40(2):459. Available from: http://www.jneurosci.org/content/40/2/459.abstract
9. Rousseaux MWC, Shulman JM, Jankovic J. Progress toward an integrated understanding of Parkinson's disease [version 1; peer review: 2 approved]. F1000Research. 2017;6(1121). Available from: http://openr.es/9uu
10. Campêlo CL das C, Silva RH. Genetic Variants in SNCA and the Risk of Sporadic Parkinson's Disease and Clinical Outcomes: A Review. Parkinsons Dis. 2017/07/11. 2017;2017:4318416. Available from: https://pubmed.ncbi.nlm.nih.gov/28781905
11. Singleton AB, Farrer M, Johnson J, Singleton A, Hague S, Kachergus J, et al. α-Synuclein Locus Triplication Causes Parkinson's Disease. Science (80-). 2003;302(5646):841. Available from: http://science.sciencemag.org/content/302/5646/841.abstract
12. Gründemann J, Schlaudraff F, Haeckel O, Liss B. Elevated α-synuclein mRNA levels in individual UV-laser-microdissected dopaminergic substantia nigra neurons in idiopathic Parkinson's disease . Nucleic Acids Res. 2008 Mar 10;36(7):e38–e38. Available from: https://doi.org/10.1093/nar/gkn084
13. Feany MB, Bender WW. A Drosophila model of Parkinson's disease. Nature. 2000;404(6776):394–8. Available from: https://doi.org/10.1038/35006074
14. Masliah E, Rockenstein E, Veinbergs I, Mallory M, Hashimoto M, Takeda A, et al. Dopaminergic Loss and Inclusion Body Formation in α-Synuclein Mice: Implications for Neurodegenerative Disorders. Science (80-). 2000;287(5456):1265. Available from: http://science.sciencemag.org/content/287/5456/1265.abstract
15. Lakso M, Vartiainen S, Moilanen A-M, Sirviö J, Thomas JH, Nass R, et al. Dopaminergic neuronal loss and motor deficits in Caenorhabditis elegans overexpressing human α-synuclein. J Neurochem. 2003 Jul 1;86(1):165–72. Available from: https://doi.org/10.1046/j.1471-4159.2003.01809.x
16. Chu Y, Kordower JH. Age-associated increases of α-synuclein in monkeys and humans are associated with nigrostriatal dopamine depletion: Is this the target for Parkinson's disease? Neurobiol Dis. 2007;25(1):134–49. Available from: http://www.sciencedirect.com/science/article/pii/S0969996106002191
17. Polymeropoulos MH, Lavedan C, Leroy E, Ide SE, Dehejia A, Dutra A, et al. Mutation in the alpha-synuclein gene identified in families with Parkinson's disease. Science. 1997 Jun;276(5321):2045–7.
18. Stefanis L. α-Synuclein in Parkinson's Disease. Cold Spring Harb Perspect Med . 2012 Feb 1;2(2). Available from: http://perspectivesinmedicine.cshlp.org/content/2/2/a009399.abstract
19. Sulzer D, Edwards RH. The physiological role of α-synuclein and its relationship to Parkinson's Disease. J Neurochem. 2019 Sep 1;150(5):475–86. Available from: https://doi.org/10.1111/jnc.14810

20. Becket G-H, Manuela P, Megumi M-T, Ling D, M. WA, H. NE, et al. αβγ-Synuclein triple knockout mice reveal age-dependent neuronal dysfunction. Proc Natl Acad Sci. 2010 Nov 9;107(45):19573–8. Available from: https://doi.org/10.1073/pnas.1005005107
21. Kokhan VS, Afanasyeva MA, Van'kin GI. α-Synuclein knockout mice have cognitive impairments. Behav Brain Res. 2012;231(1):226–30.
22. Rousseaux MWC, Vázquez-Vélez GE, Al-Ramahi I, Jeong H-H, Bajić A, Revelli J-P, et al. A Druggable Genome Screen Identifies Modifiers of α-Synuclein Levels via a Tiered Cross-Species Validation Approach. J Neurosci. 2018;38(43):9286. Available from: http://www.jneurosci.org/content/38/43/9286.abstract
23. Shu F, Lv S, Qin Y, Ma X, Wang X, Peng X, et al. Functional characterization of human PFTK1 as a cyclin-dependent kinase. Proc Natl Acad Sci U S A. 2007/05/21. 2007 May 29;104(22):9248–53. Available from: https://pubmed.ncbi.nlm.nih.gov/17517622
24. Chen L, Wang Y, Jiang W, Ni R, Wang Y, Ni S. CDK14 involvement in proliferation migration and invasion of esophageal cancer. Ann Transl Med. 2019 Nov;7(22):681. Available from: https://pubmed.ncbi.nlm.nih.gov/31930082
25. Zhou Y, Rideout WM, Bressel A, Yalavarthi S, Zi T, Potz D, et al. Spontaneous genomic alterations in a chimeric model of colorectal cancer enable metastasis and guide effective combinatorial therapy. PLoS One. 2014;9(8):1–13.
26. Ferguson FM, Doctor ZM, Ficarro SB, Browne CM, Marto JA, Johnson JL, et al. Discovery of Covalent CDK14 Inhibitors with Pan-TAIRE Family Specificity. Cell Chem Biol. 2019;26(6):804-817.e12. Available from: http://www.sciencedirect.com/science/article/pii/S2451945619300704
27. Rodríguez González Y, Kamkar F, Jafar-nejad P, Wang S, Qu D, Sanchez Alvarez L, et al. PFTK1 kinase regulates axogenesis during development via RhoA activation. bioRxiv. 2022 Jan 1;2022.01.11.475789. Available from: http://biorxiv.org/content/early/2022/03/10/2022.01.11.475789.abstract
28. Kuo Y-M, Li Z, Jiao Y, Gaborit N, Pani AK, Orrison BM, et al. Extensive enteric nervous system abnormalities in mice transgenic for artificial chromosomes containing Parkinson disease-associated alpha-synuclein gene mutations precede central nervous system changes. Hum Mol Genet. 2010/01/27. 2010 May 1;19(9):1633–50. Available from: https://pubmed.ncbi.nlm.nih.gov/20106867
29. Volpicelli-Daley LA, Luk KC, Patel TP, Tanik SA, Riddle DM, Stieber A, et al. Exogenous α-synuclein fibrils induce Lewy body pathology leading to synaptic dysfunction and neuron death. Neuron. 2011 Oct 6;72(1):57–71. Available from: https://pubmed.ncbi.nlm.nih.gov/21982369
30. Polinski NK, Volpicelli-Daley LA, Sortwell CE, Luk KC, Cremades N, Gottler LM, et al. Best Practices for Generating and Using Alpha-Synuclein Pre-Formed Fibrils to Model Parkinson's Disease in Rodents. J Parkinsons Dis. 2018;8(2):303–22. Available from: https://pubmed.ncbi.nlm.nih.gov/29400668
31. Deacon R. Assessing burrowing, nest construction, and hoarding in mice. J Vis Exp. 2012 Jan 5;(59):e2607–e2607. Available from: https://pubmed.ncbi.nlm.nih.gov/22258546
32. Geertsma HM, Suk TR, Ricke KM, Horsthuis K, Parmasad J-LA, Fisk ZA, et al. Constitutive nuclear accumulation of endogenous alpha-synuclein in mice causes motor impairment and cortical dysfunction, independent of protein aggregation. Hum Mol Genet. 2022 Feb 18;ddac035. Available from: https://doi.org/10.1093/hmg/ddac035
33. Soldner F, Laganière J, Cheng AW, Hockemeyer D, Gao Q, Alagappan R, et al.

850 Generation of Isogenic Pluripotent Stem Cells Differing Exclusively at Two Early Onset
851 Parkinson Point Mutations. Cell. 2011;146(2):318–31. Available from:
852 https://www.sciencedirect.com/science/article/pii/S0092867411006611
853 34. Ryan SD, Dolatabadi N, Chan SF, Zhang X, Akhtar MW, Parker J, et al. Isogenic Human
854 iPSC Parkinson's Model Shows Nitrosative Stress-Induced Dysfunction in MEF2-PGC1α
855 Transcription. Cell. 2013;155(6):1351–64. Available from:
856 http://www.sciencedirect.com/science/article/pii/S0092867413014220
857 35. Kriks S, Shim J-W, Piao J, Ganat YM, Wakeman DR, Xie Z, et al. Dopamine neurons
858 derived from human ES cells efficiently engraft in animal models of Parkinson's disease.
859 Nature. 2011;480(7378):547–51. Available from: https://doi.org/10.1038/nature10648
860 36. Delaney SP, Julian LM, Pietrobon A, Yockell-Lelièvre J, Doré C, Wang TT, et al. Human
861 pluripotent stem cell modeling of tuberous sclerosis complex reveals lineage-specific
862 therapeutic vulnerabilities. bioRxiv. 2020 Jan 1;683359. Available from:
863 http://biorxiv.org/content/early/2020/02/14/683359.abstract
864 37. Tomlinson JJ, Shutinoski B, Dong L, Meng F, Elleithy D, Lengacher NA, et al.
865 Holocranohistochemistry enables the visualization of α-synuclein expression in the murine
866 olfactory system and discovery of its systemic anti-microbial effects. J Neural Transm.
867 2017;124(6):721–38. Available from: https://doi.org/10.1007/s00702-017-1726-7
868 38. Bojan S, Mansoureh H, E. HI, Michaela L, Juliana R, Nathalie L, et al. Lrrk2 alleles
869 modulate inflammation during microbial infection of mice in a sex-dependent manner. Sci
870 Transl Med. 2019 Sep 25;11(511):eaas9292. Available from:
871 https://doi.org/10.1126/scitranslmed.aas9292
872 39. Volpicelli-Daley LA, Luk KC, Lee VM-Y. Addition of exogenous α-synuclein preformed
873 fibrils to primary neuronal cultures to seed recruitment of endogenous α-synuclein to
874 Lewy body and Lewy neurite–like aggregates. Nat Protoc. 2014;9(9):2135–46. Available
875 from: https://doi.org/10.1038/nprot.2014.143
876 40. Luk KC, Kehm V, Carroll J, Zhang B, O'Brien P, Trojanowski JQ, et al. Pathological α-
877 Synuclein Transmission Initiates Parkinson-like Neurodegeneration in Nontransgenic
878 Mice. Science (80-). 2012;338(6109):949. Available from:
879 http://science.sciencemag.org/content/338/6109/949.abstract
880 41. Mao X, Ou MT, Karuppagounder SS, Kam T-I, Yin X, Xiong Y, et al. Pathological α-
881 synuclein transmission initiated by binding lymphocyte-activation gene 3. Science. 2016
882 Sep 30;353(6307):aah3374. Available from: https://pubmed.ncbi.nlm.nih.gov/27708076
883 42. Kam T-I, Mao X, Park H, Chou S-C, Karuppagounder SS, Umanah GE, et al. Poly(ADP-
884 ribose) drives pathologic α-synuclein neurodegeneration in Parkinson's disease. Science.
885 2018 Nov 2;362(6414):eaat8407. Available from:
886 https://pubmed.ncbi.nlm.nih.gov/30385548
887 43. Hallam RD, Buchner-Duby B, Stykel MG, Coackley CL, Ryan SD. Intracellular
888 Accumulation of α-Synuclein Aggregates Promotes S-Nitrosylation of MAP1A Leading
889 to Decreased NMDAR-Evoked Calcium Influx and Loss of Mature Synaptic Spines. J
890 Neurosci. 2022 Dec 14;42(50):9473 LP – 9487. Available from:
891 http://www.jneurosci.org/content/42/50/9473.abstract
892 44. Bhullar KS, Lagarón NO, McGowan EM, Parmar I, Jha A, Hubbard BP, et al. Kinase-
893 targeted cancer therapies: progress, challenges and future directions. Mol Cancer. 2018
894 Feb 19;17(1):48. Available from: https://pubmed.ncbi.nlm.nih.gov/29455673
895 45. Gouda NA, Elkamhawy A, Cho J. Emerging Therapeutic Strategies for Parkinson's

Disease and Future Prospects: A 2021 Update. Vol. 10, Biomedicines. 2022.
46. L. BE, Aaron M, D. SK, S. BK, Mastooreh C, E. MT, et al. Alpha-Synuclein Expression Restricts RNA Viral Infections in the Brain. J Virol. 2022 May 2;90(6):2767–82. Available from: https://doi.org/10.1128/JVI.02949-15
47. Allen Reish HE, Standaert DG. Role of α-synuclein in inducing innate and adaptive immunity in Parkinson disease. J Parkinsons Dis. 2015;5(1):1–19. Available from: https://pubmed.ncbi.nlm.nih.gov/25588354
48. Rousseaux MWC, de Haro M, Lasagna-Reeves CA, De Maio A, Park J, Jafar-Nejad P, et al. TRIM28 regulates the nuclear accumulation and toxicity of both alpha-synuclein and tau. Ackerman SL, editor. Elife. 2016;5:e19809. Available from: https://doi.org/10.7554/eLife.19809
49. Rousseaux MWC, Revelli J-P, Vázquez-Vélez GE, Kim J-Y, Craigen E, Gonzales K, et al. Depleting Trim28 in adult mice is well tolerated and reduces levels of α-synuclein and tau. Ackerman SL, editor. Elife. 2018;7:e36768. Available from: https://doi.org/10.7554/eLife.36768
50. Karczewski KJ, Francioli LC, Tiao G, Cummings BB, Alföldi J, Wang Q, et al. The mutational constraint spectrum quantified from variation in 141,456 humans. Nature. 2020;581(7809):434–43. Available from: https://doi.org/10.1038/s41586-020-2308-7
51. Sorrentino ZA, Vijayaraghavan N, Gorion K-M, Riffe CJ, Strang KH, Caldwell J, et al. Physiological C-terminal truncation of α-synuclein potentiates the prion-like formation of pathological inclusions. J Biol Chem. 2018;293(49):18914–32. Available from: https://www.sciencedirect.com/science/article/pii/S0021925820311297
52. Ma L, Yang C, Zhang X, Li Y, Wang S, Zheng L, et al. C-terminal truncation exacerbates the aggregation and cytotoxicity of α-Synuclein: A vicious cycle in Parkinson's disease. Biochim Biophys Acta - Mol Basis Dis. 2018;1864(12):3714–25. Available from: https://www.sciencedirect.com/science/article/pii/S0925443918303806
53. Tofaris GK, Reitböck PG, Humby T, Lambourne SL, O'Connell M, Ghetti B, et al. Pathological Changes in Dopaminergic Nerve Cells of the Substantia Nigra and Olfactory Bulb in Mice Transgenic for Truncated Human α-Synuclein(1–120): Implications for Lewy Body Disorders. J Neurosci. 2006 Apr 12;26(15):3942 LP – 3950. Available from: http://www.jneurosci.org/content/26/15/3942.abstract
54. Moors TE, Maat CA, Niedieker D, Mona D, Petersen D, Timmermans-Huisman E, et al. The subcellular arrangement of alpha-synuclein proteoforms in the Parkinson's disease brain as revealed by multicolor STED microscopy. Acta Neuropathol. 2021;142(3):423–48. Available from: https://doi.org/10.1007/s00401-021-02329-9
55. Zhang M, Zhang L, Geng A, Li X, Zhou Y, Xu L, et al. CDK14 inhibition reduces mammary stem cell activity and suppresses triple negative breast cancer progression. Cell Rep. 2022;40(11):111331. Available from: https://www.sciencedirect.com/science/article/pii/S2211124722011597

938 **Figures**

939 **Figure 1. Loss of Cdk14 ameliorates grip strength impairment and α-Syn pathology in PFF-**
940 **injected mice.** (A) Mouse α-Syn PFFs were injected unilaterally into the striatum by stereotactic
941 injection in 6-month-old mice. (B) Loss of forelimb grip strength at 6 months post α-Syn PFF-
942 treatment in WT mice, but not in *Cdk14*$^{+/-}$ or *Cdk14*$^{-/-}$ mice. Mean + SEM, two-way ANOVA,
943 Bonferroni *post hoc,* n: 9-10. (C) α-Syn PFF-injection increased the load of pS129 α-Syn-positive
944 cells (depicted without and with hematoxylin counterstaining, 50 µm scale bars) in the injected
945 hemisphere (ipsilateral, IL; injection site indicated by *). Densities of pS129 α-Syn-positive cells
946 are represented in heat maps as hues of red at 3 rostrocaudal levels (relative to bregma: +0.98 mm,
947 +0.26 mm, and -1.34 mm) with dark shades of red correlating to high cell densities (injection sites
948 marked by asterisks). Amounts of pS129 α-Syn-positive cells in all brain regions (averaged in IL
949 and contralateral to the injection, CL), the somatomotor cortex and the striatum at +0.26 mm
950 relative to bregma of PFF-injected *Cdk14*$^{+/-}$ and *Cdk14*$^{-/-}$ mice were lower relative to their wildtype
951 (WT) counterparts. Mean + SEM, two-way ANOVA, Bonferroni *post hoc* comparisons, n: 3-6.
952 (D) PFF injection reduces the tyrosine hydroxylase (TH)-positive fiber density IL in comparison
953 to the non-injected hemisphere (CL) to a similar degree in WT, *Cdk14*$^{+/-}$ and *Cdk14*$^{-/-}$ mice at
954 +0.26 mm relative to bregma (200 µm scale bar). Mean + SEM, two-way ANOVA, Bonferroni
955 *post hoc* comparisons, n: 3-7.

956

957 **Figure 2. Primary cortical neurons lacking Cdk14 exhibit decreased spreading of seed-**
958 **competent α-Syn**

959 (A) Paradigm for passaging PFF-transduced WT, *Cdk14*$^{+/-}$, and *Cdk14*$^{-/-}$ primary culture media to
960 WT, naïve cultures. Media from 21 DIV cultures transduced with PFFs for 14 days were collected,

961 filtered, and added to naïve cultures at 7 DIV. Media-treated cultures were then fixed and analyzed
962 for fluorescent pS129 α-Syn signal. (B) Conditioned media from *Cdk14*$^{+/-}$ and *Cdk14*$^{-/-}$ neurons
963 induce less α-Syn pathology (indicated by pS129 α-Syn-positive area) in naïve WT neurons
964 compared to WT conditioned media (50 µm scale bars). Mean + SEM, two-way ANOVA, Holm-
965 Šídák post hoc comparisons, n=4.

966

967 **Figure 3. Genetic reduction of Cdk14 attenuates pS129 α-Syn in human neurons.**
968 Immunoblots illustrating elevated amounts of pS129 α-Syn in the RIPA buffer-soluble protein
969 fraction of hiPSC-derived *SNCA* A53T human neurons (in comparison to isogenic corrected
970 neurons [Corr]) which is reduced by CRISPR/Cas9-mediated knockdown of *CDK14* (targeted
971 against *CDK14* exon 3 (E3) and 8 (E8), NT non-targeting control). Mean + SEM, one-way
972 ANOVA, Tukey *post hoc* comparisons, n=3-4.

973

974 **Figure 4. Pharmacological inhibition of CDK14 reduces α-Syn protein burden in human and**
975 **rodent neurons.** (A) Dose-dependent reduction of α-Syn in hESC-derived human neurons is
976 detected by ELISA-quantification after 6 days of CDK14 inhibitor FMF-04-159-2 treatment. Mean
977 + SEM, one-way ANOVA, Bonferroni *post hoc* comparisons, n=3. (B) Human α-Syn PFFs applied
978 to rat cortical neurons for 5 days increase the amounts of α-Syn and CDK14 in the insoluble protein
979 fraction (Urea buffer-soluble) compared to untreated (UT) and α-Syn monomers (Mono)-treated
980 neurons, as shown by immunoblots, which were reduced by the application of 100 nM of the
981 CDK14 inhibitor. Mean + SEM, two-way ANOVA, Holm-Šídák *post hoc* comparisons, n=3.

982

983 **Figure 5. Inhibition of Cdk14 decreases human α-Syn protein in mice expressing A53T**
984 ***SNCA*.** (A) Intracerebroventricular (ICV) administration strategy for the CDK14 inhibitor FMF-
985 04-159-2 at 0.35 mg/kg/day for 28 days in 4-month-old *PAC α-Syn*^{A53T} *TG* mice. (B) Immunoblots
986 with protein isolated from the brain of FMF-04-159-2-treated *PAC α-Syn*^{A53T} *TG* mice visualize
987 the reduction of α-Syn in the TSS buffer-soluble, Cdk14 in the TXS buffer and SDS buffer-soluble
988 and C-terminally truncated (CTT) α-Syn (arrowhead at high exposure (high exp.)) in the TSS
989 buffer- and TXS buffer-soluble protein fraction in comparison to vehicle-treated mice. Mean +
990 SEM, unpaired student's *t* test, n=6.
991
992
993
994
995
996
997
998
999
1000
1001
1002
1003
1004
1005

Fig. 1

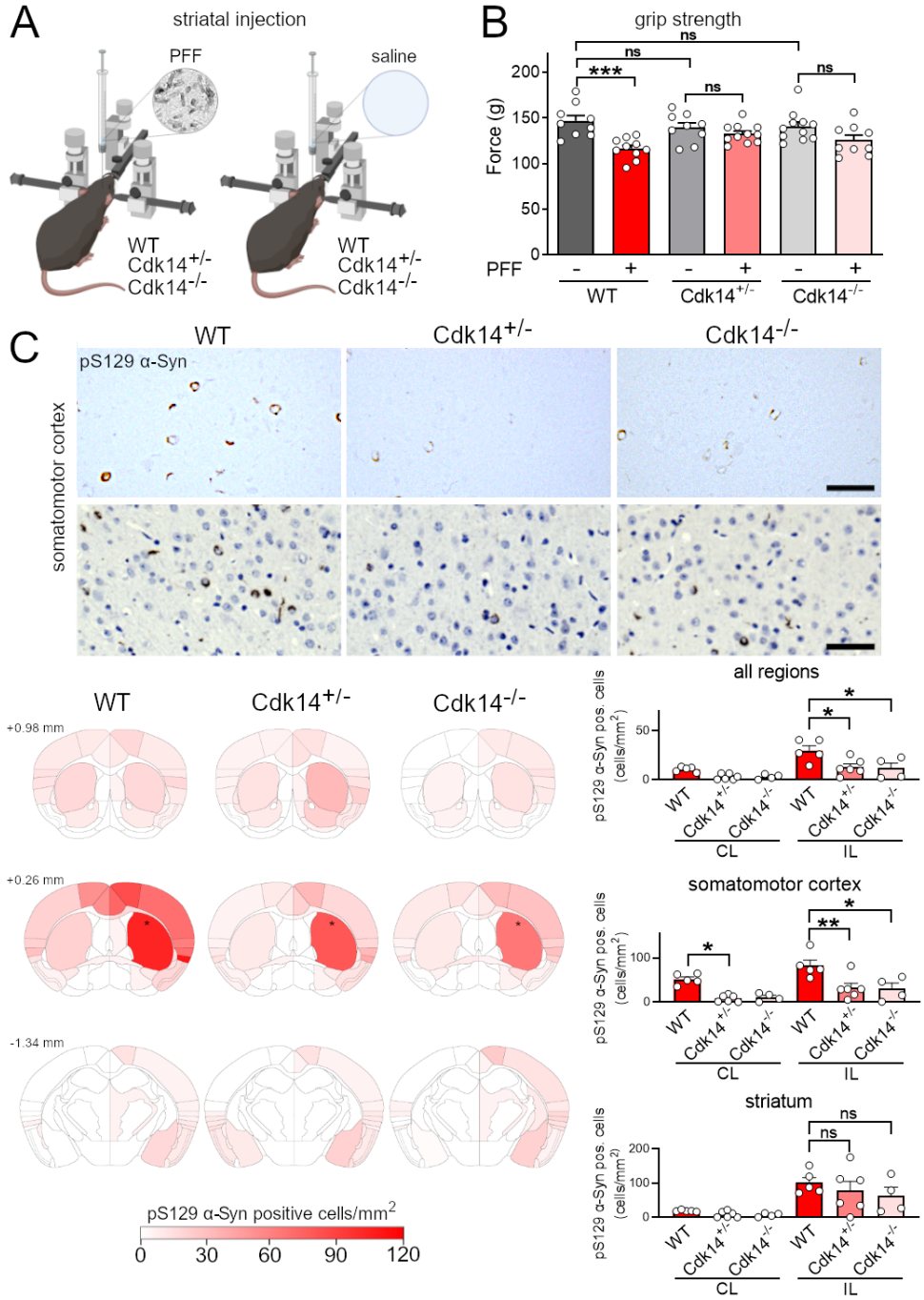
A
striatal injection
PFF
saline
WT
Cdk14+/-
Cdk14-/-
B
grip strength
Force (g)
PFF
WT
Cdk14+/-
Cdk14-/-
C
pS129 α-Syn
somatomotor cortex
+0.98 mm
+0.26 mm
-1.34 mm
pS129 α-Syn positive cells/mm2
all regions
somatomotor cortex
striatum
pS129 α-Syn pos. cells (cells/mm2)
CL
IL
D
+0.26 mm
TH
saline
PFF
striatal TH
striatal TH intensity (% of CL)

1008

1009 **Fig. 2**

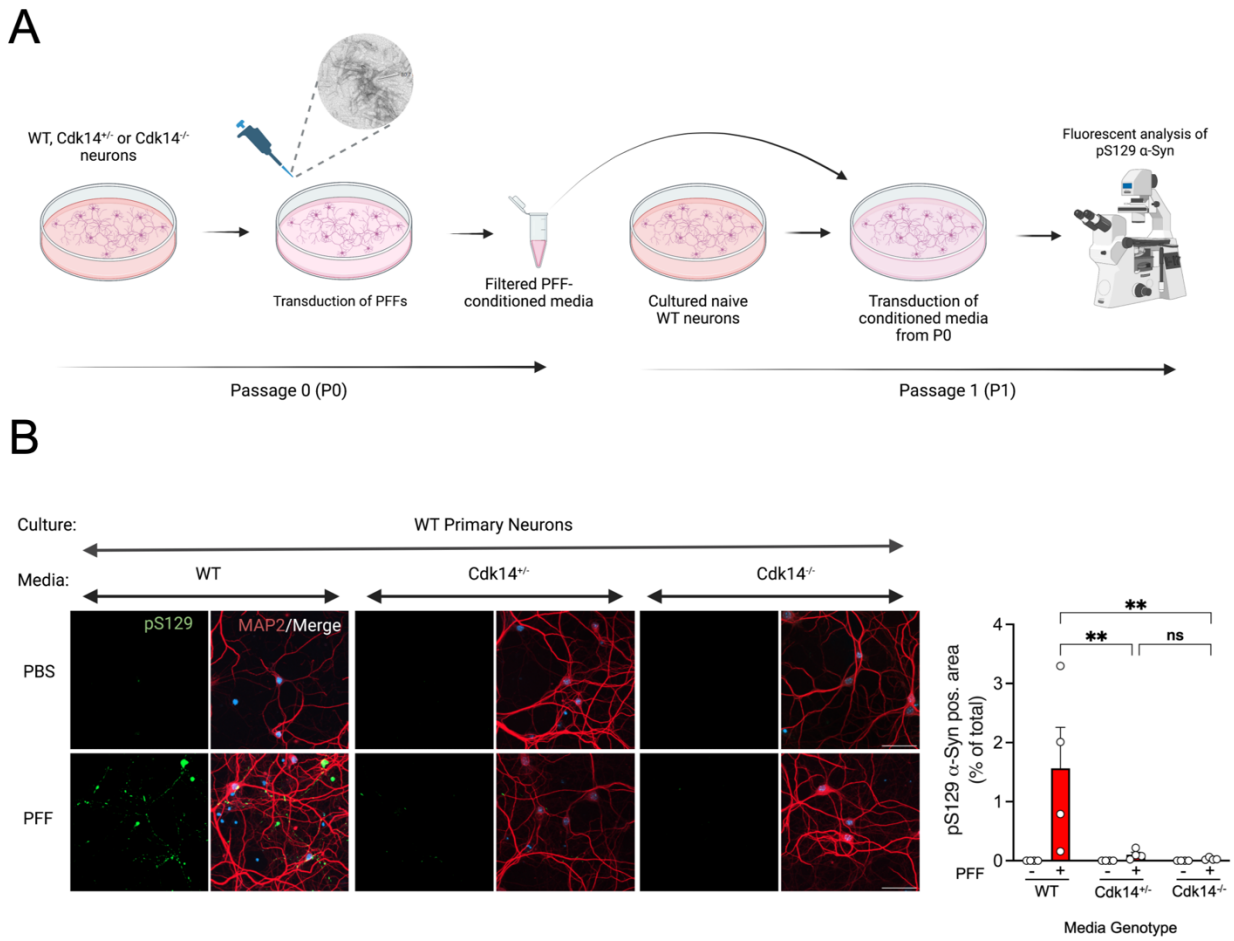

1010

1011

1012

1013

1014

1015

1016

1017

1018

1019 **Fig. 3**

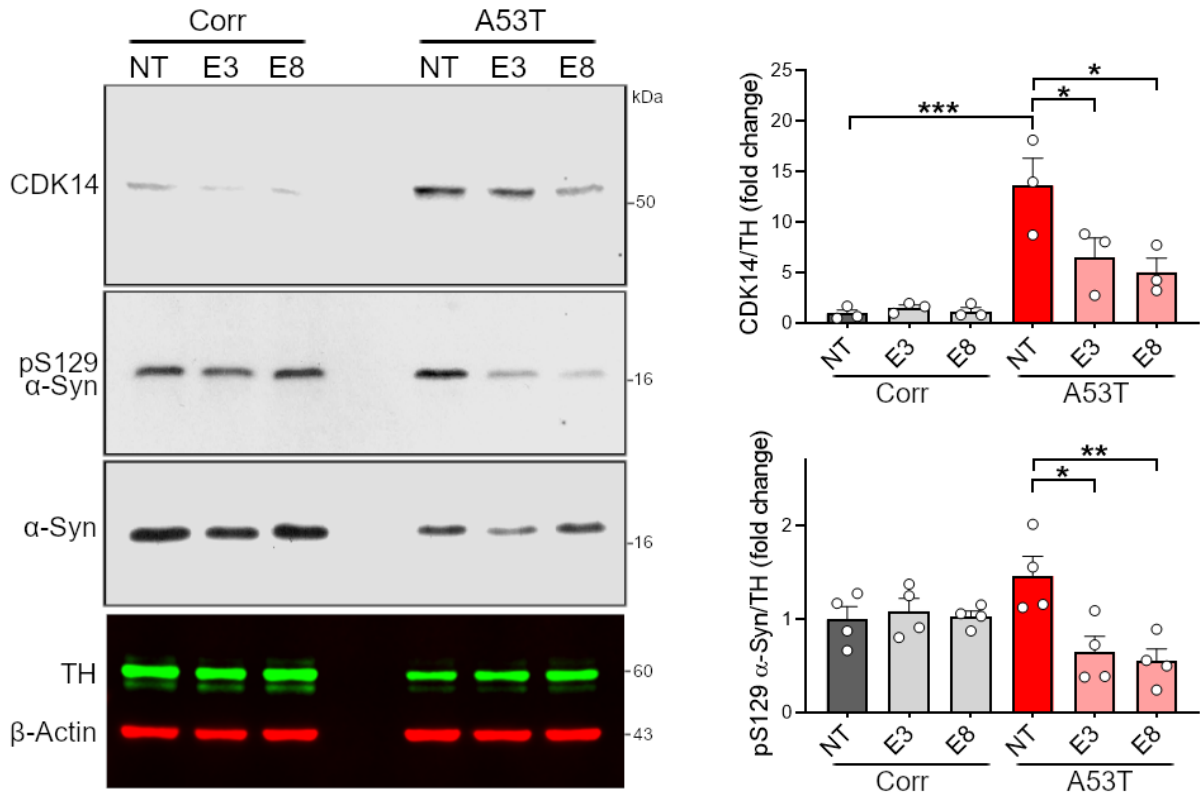

1020

1021

1022

1023

1024

1025

1026

1027

1028

1029

1030

1031

1032 **Fig. 4**

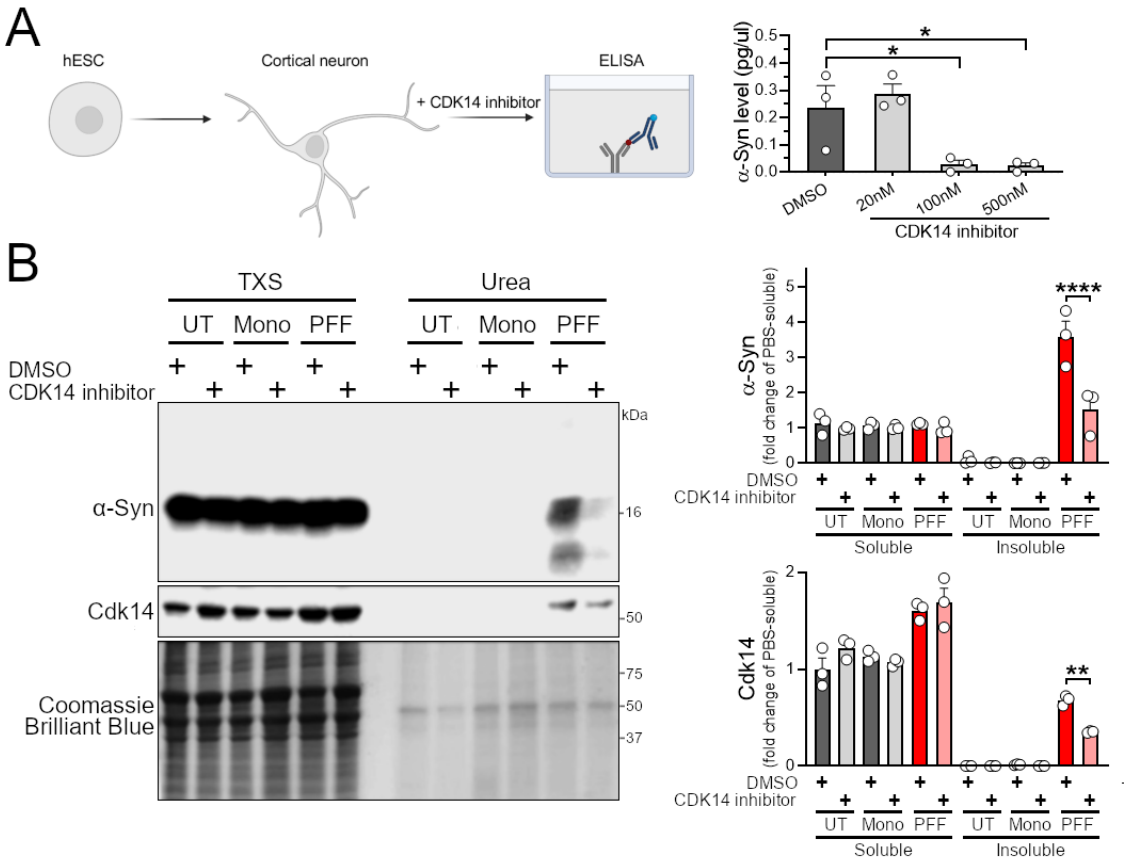

1033

1034 **Fig. 5**

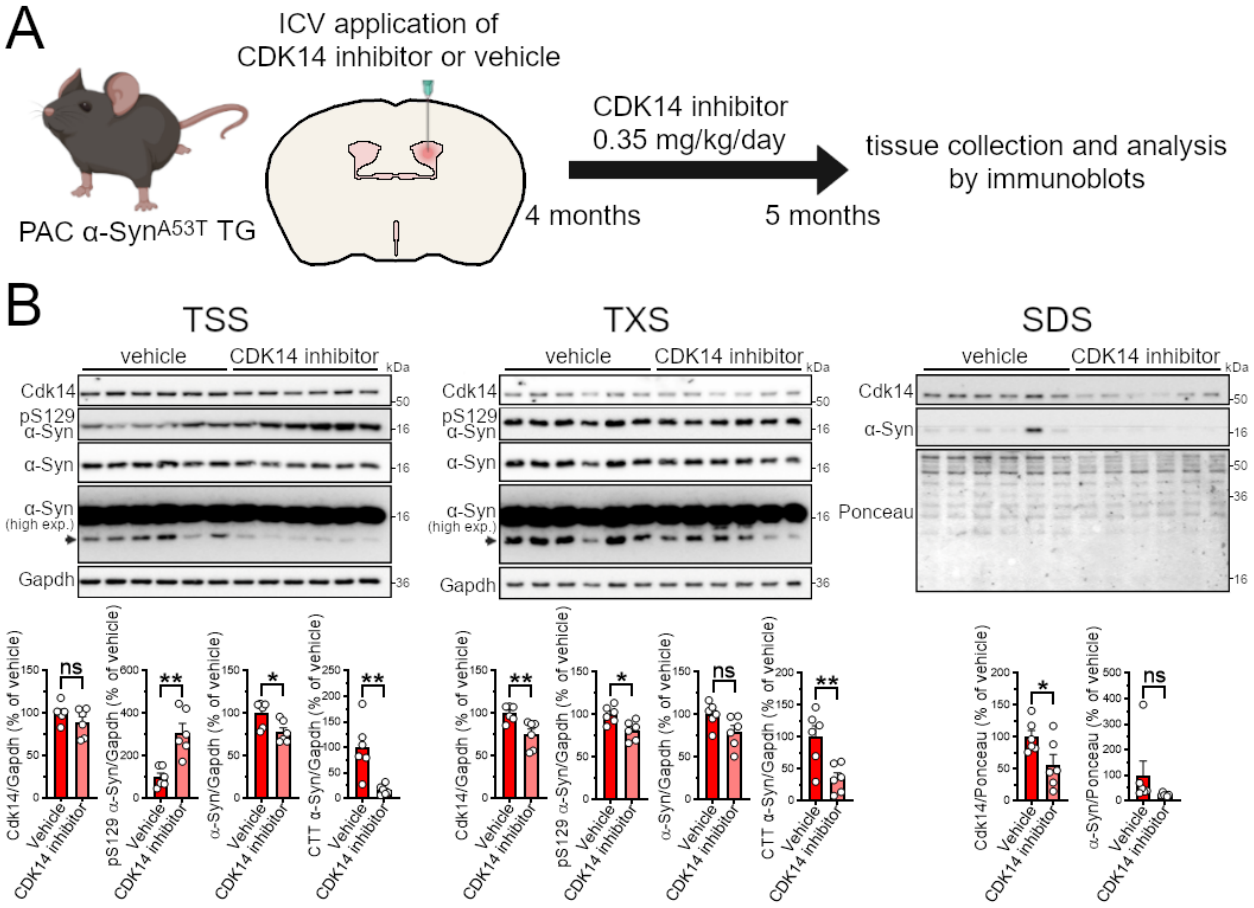

1035

1036